Tunneling and THz Spectroscopy Study Through the Disordered-Tuned Superconductor-Insulator Transition

Daniel Sherman

May 25, 2015

Acknowledgments

I would like to express my deepest gratitude and appreciation to my advisor, Aviad Frydman. He continually and convincingly conveyed a spirit of adventure in regard to research. Without his guidance and persistent help this dissertation would not have been possible. Thank you for your unconditional support in so many aspects.

I would like to thank my fellow lab members, past and present: Ora Biton, Tal Havdala, Noa Kurzweil, Ariel Eisenbach, Nati Ossi. I would like to specifically thank my friend and colleague Shahaf Poran.

I would like to acknowledge and thank Martin Dressel for his support and good advisement, specifically in the THz spectroscopy measurements which were performed at his lab in Stuttgart university. Thank you for always making me feel welcome. I wish to thank Boris Gorshunov for his endless patient and support in teaching me all the THz system secrets. I also owe to Uwe Pracht for his support during the long THz measurements.

I would like to thank Danny Shahar for his support in the tunneling measurements.

I would also like to acknowledge and thank Eli Farber for helping me reach the goals I pursued.

I wish to acknowledge the many useful discussions I had with Nandini Trivedi, Efrat Shimshoni, Assa Auerbach, Pratap Raychaudhuri and many others.

Last but not least, I would like to thank my family. Yael, my love and my wife, thank you for your support. Ron, our son, soon you will be able to read this, thank you; may you allow us to keep you as happy as you make us.

Contents

List of Figures

List of Abbreviations

NbN Niobium Nitride
InO Indium Oxide
SIT Superconductor to Insulator Transition
d-SIT Disorder driven SIT
THz Terahertz
ZBA Zero Bias Anomaly
BWO Backward Wave Oscillator
QPT Quantum Phase Transition

Abstract

The interplay between disorder and superconductivity is a fundamental research field in condense matter physics and it is the subject of this current thesis. While increasing disorder tends to localize the electronic wave function, superconductivity tends to the opposite by forming a macroscopically coherent many-body state of Cooper pairs. The current thesis focuses on systems in which increasing disorder suppresses the superconducting ground state and signals the appearance of an insulating ground state; this is called the disorder driven superconductor to insulator transition (d-SIT). The d-SIT, being driven by a non thermodynamical parameter, manifests a prototype of a quantum phase transition, which is on its own a fundamental research field. Increasing interest in the field of the SIT in general and the d-SIT in particular, during the last three decades yielded many experimental and theoretical results (which will be reviewed in chapter 1). However, a detailed description of the disorder effects on superconductors and the ultimate destruction of superconductivity at higher degrees of disorder remains elusive and controversial. Moreover, once the SIT is achieved the detailed physical description depends on the system of choice and on the tuning parameter of the phase transition. In principle the systems can be divided to two types: structurally granular and structurally uniform or homogeneous systems. Introducing disorder, however, ultimately generates a characteristic structural inhomogeneity length scale. The distinction between the two types of systems can be understood by the ability of an individual region defined by the latter length scale to sustain superconductivity. In the current thesis we study uniform systems, namely homogeneously disordered indium oxide (InO) thin films and niobium nitride (NbN) thin films. These systems are indeed structurally homogeneous, however, at low temperatures they share many electrical properties with granular systems. The breakdown to non-homogeneous electrical behavior is not shared by all homogeneous systems with a superconducting ground state; thus the description of the studied system should include more details than merely the structural properties. A possible additional key ingredient to properly classify the systems is the electron carrier density. For both InO and NbN systems employed here the electron carrier density is significantly lower than the case of normal metals.

Practically, the d-SIT can be tuned in various methods. Our prime tuning parameters of the d-SIT are varying the system chemical composition, which is determined during the films deposition process, and reducing the static disordered potential by sequences of annealing processes. Another method to drive the d-SIT is by varying the thickness of the film.

We performed a number of experimental methods designed to study the behaviour of the superconducting energy gap, Δ, through the d-SIT. First, we performed tunneling measurements on insulating and superconducting InO thin films. Surprisingly, the tunneling density of states of the insulating sample was similar to the superconducting sample; specifically, a superconducting energy gap appeared in the insulating sample. Moreover, the value of the superconducting energy gap, extracted from the tunneling spectra of both of these systems, was found to be almost identical. The existence of such superconducting correlations in a sample that macroscopically exhibits an insulating behaviour implies that electrical inhomogeneity exists over small length scales in these structurally homogeneous films. In fact, this is exactly the situation in structurally granular films.

A second experimental method we employed was Terahertz (THz) optical spectroscopy. We performed measurements on thin films of NbN and InO with different degrees of disorder spanning the d-SIT. Traditionally the conductivity of disordered s-wave superconductors was probed by

various dc measurements; though, recently a few groups employed microwave measurements which essentially probe frequencies below the superconducting energy gap. In this respect, the THz optical spectroscopy provides a novel experimental approach to the research field of the d-SIT. This well known optical measurement is frequently employed in various fields such as high-Tc superconductors, however, it was never used to study disordered s-wave superconductors, particularly near the quantum phase transition. Based on the fact that the dc and the optical measurements essentially probe different physical quantities, though both are ultimately linked to the same models, comparing their results is bound to yield new insights on the physical nature of the d-SIT. Indeed, one example stemming from such a comparison is the observation that Coulomb interactions play a major role in disorder superconductors near the d-SIT. In fact, we were able to show that the SIT itself may be tuned by varying the strength of Coulomb interactions.

The photon energy spectrum of the THz system covers the vicinity of the superconducting energy gap, thus allowing to directly measure its value. Indeed we observed the superconducting gap develops as expected from the BCS theory on superconducting NbN films far from the d-SIT. However, with increasing disorder and approaching quantum criticality, both superconducting films of NbN and InO exhibit significant deviation from the BCS expressions and from corresponding tunneling measurements. Optical spectroscopy is sensitive to the lowest energy excitation mechanism. Hence, these results indicate that another mechanism sets in at energies lower than the superconducting energy gap. We attribute this mechanism to amplitude collective modes, also known as the Higgs mode (relevant in high energy physics). This experimental result is found to be in good agreement with recent theoretical calculations of the Higgs mode near quantum criticality.

Chapter 1

Introduction

Since the early days of solid state physics a detailed physical description was developed for crystalline materials. However, in reality crystallites are the exception rather than the rule. Disorder exists in various degrees, ranging from a few impurities to glassy structures. The theoretical models for the electronic properties of solids stemming from ordered materials (e.g. Boltzmann transport equation) failed to describe disordered materials, emphasizing the necessity for a new approach. According to the traditional view, impurities or spatial random potential variation increases the scattering rate and reduces the mean free path, however, the electrons wave function remains extended over the entire sample. In 1958, Anderson[1] showed that quantum diffusion of electrons in a random potential is suppressed due to interference effects. In other words, increasing disorder spatially localizes the electronic wave function in the vicinity of the Fermi level, so that the electronic wave function Ψ follows $|\Psi| \sim exp(|r - r_0|/\xi)$, where ξ is the localization length. Consequently, at some critical degree of disorder, dc conductivity at zero temperature is impossible, thus forming an insulating ground state, known as Anderson insulator. The existence of such localized electronic states around the Fermi energy distinguishes Anderson insulator from band insulator. In the latter case the highest occupied energy band formed in an ordered material is completely full. In order to conduct, such a band insulator requires an energy equal to the difference between the occupied band and the next unoccupied band. About ten years later, Mott[2] introduced the concept of mobility edge which separates energetically the localized states from the extended states. The relative location of the mobility edge (E_c) compared to the Fermi energy (E_f) determines whether the system is a conductor (i.e. $E_f > E_c$) or an insulator (i.e. $E_f < E_c$). At low temperatures, Anderson insulators conduct by hopping mechanism, where the electrons hop or tunnel between localized states. The latter mechanism is also known as variable range hopping (VRH). The temperature dependence of the resistance in the VRH regime is characterized as follow:

$$R(T) = R_0 exp(T_0/T)^{\nu} \tag{1.1}$$

where R_0 is a prefactor, T_0 is a characteristic temperature and ν is a characteristic exponent the value of which distinguishes different conduction mechanism. Since the hopping conduction occurs between localized states around the Fermi level, the details of the density of states around it is an important consideration in determining the temperature dependence of resistance. Mott[3, 4] considered a constant density of states and showed that $\nu = 1/d+1$, where d is the dimensionality of the system and $T_0 = 3/k_B N(E_f)\xi^2$, where k_B is Boltzmann constant, $N(E_f)$ is the density of states near the Fermi energy and ξ is the localization length. Efros and Shklovskii[5] showed that Mott's a priori assumption of a constant $N(E_f)$ is not applicable if Coulomb interactions between the electrons are taken into account. They showed that at low temperatures Coulomb interactions cause a depletion in $N(E_f)$. Subsequently they derived a different value for the characteristic exponent of Eq.1.1: $\nu = 1/2$, which does not depend on dimensionality, and a characteristic temperature: $T_0 = 2.8e^2/4\pi\epsilon k_B\xi$, where ϵ is the material's dielectric constant. In general the theory of electron-electron interactions in disordered systems was adequately derived only in the two extreme limits. In the high disorder limit Efros and Shklovskii showed that the suppression in the density of states, known as the Coulomb gap, depends on the systems dimensionality and follows:

$$D = 2 : \delta N \sim |V| \tag{1.2}$$

$$D = 3 : \delta N \sim V^2 \tag{1.3}$$

Where the reference point for the energy V is the Fermi level. In the weak disorder limit the electrons are not localized, however, Coulomb interactions modify the electronic properties. Altshuler and Aronov[6] calculated a logarithmic corrections for the conductivity, i.e. $R \sim lnT$, and for the density of states[1]:

$$\delta N \sim -ln(V) \tag{1.4}$$

An important milestone in the research of disorder electronic systems is the scaling theory. The essential hypothesis of the scaling theory is that close to the transition between localized and extended states, there is only one relevant scaling variable. This variable is sufficient to describe the critical behavior of the dc conductivity on the metallic side and the localization length on the insulating side. According to the scaling theory, in two dimension or lower and at large enough length scales, only localized behavior is possible. A detailed description of the scaling theory is beyond the scope of the current work and can be found elsewhere, e.g. ref.[7] and references therein.

1.1 Superconductivity and disorder

At low temperatures some materials retain a superconducting rather than a normal metal ground state. The celebrated theory that microscopically describes the superconducting phase was brought forward by Bardeen, Cooper and Shrieffer[8] (BCS). Alternatively, in the Ginzburg-Landau phenomenological theory, the superconducting state can be characterized by a complex order parameter:

$$\Psi(r) \propto \Delta exp(i\phi(r)) \tag{1.5}$$

where the value of the energy gap that develops around the Fermi energy is given by Δ and ϕ is the phase of the order parameter[2]. The rearrangement of the density of states reflects the binding of electrons from the vicinity of the Fermi energy into Cooper pairs with a binding energy of 2Δ. One important length scale in the superconducting phase is the coherence length, ξ, which roughly defines the size of the Cooper pairs and is given by: $\xi_0 \sim \hbar v_F/\Delta$, where v_F is the Fermi

[1]The exact expression for 2D, where the thermal length is larger than the thickness of the sample, can also be found in Eq.(3), paper 6.1.

[2]Rigorously, G-L theory gives $\Psi(r) = Aexp(i\phi(r))$, where $|A|^2$ is the local density of superconducting electrons, $n_s(r)$. However, Gorkov[9] showed that, in conventional s-wave superconductor, the order parameter A of the G-L theory is proportional to the pair potential or energy gap Δ. At the same time this proves that the effective charge equals $2e$ and the effective mass equals $2m$, representing the Cooper pairs from the microscopic BCS theory.

velocity. Typical values for the superconducting coherence length are in the range of a hundred nanometers. In principle, the BCS model is applicable as long as $\xi >> (g_0\Delta)^{-1/3}$, where g_0 is the density of states at the Fermi level. The effects of disorder on a system with a superconducting ground state was first studied by Anderson[10] in the late 50's. Explicitly ignoring electron-electron interaction, Anderson claimed that the introduction of nonmagnetic impurities does not lead to a substantial change in the superconducting properties and in particular the transition temperature, T_C. Experimentally, it was realized already on the 70's that increasing disorder does eventually suppress the value of T_C. Strongin et al.[11] measured the transport properties of Pb and Bi, deposited on various substrates, and found a dramatic decrease in T_C with decreasing thickness [3]. A systematic reduction in T_C as a function of thickness and/or chemical composition was later observed[13–15] in structurally uniform disordered $MoGe$ films[4]. Later, similar results were also obtained in structurally uniform films of InO [16–19], NbN [20], TiN [21] and others. In fact, the termination of the superconducting state due to increasing disorder is not limited to any specific set of systems; including structurally granular s-wave systems(e.g. ref.[22]) and high T_C superconductors (e.g. ref.[23–25]). Clearly Anderson theorem had to be modified in the case of highly disordered films. Indeed, several theoretical models for the d-SIT were brought forward over the last three decades, each model emphasize different aspects. The theoretical approaches can be divided to three: (1) Bosonic model, (2) Fermionic model and (3) induced electrical inhomogeneity. The difference between the first two fundamental models can be formulated using the complex order parameter defined in Eq. 1.5. In the absence of current the phase of the order parameter, ϕ, remains constant inside the superconductor, thus reflecting the existence of quantum correlations between the electron pairs. In the presence of fluctuations the superconducting state holds until the correlator $G(r) =< \Psi(r)\Psi(0) >$ (The angular brackets indicates averaging over the quantum state of the system) tends to a finite value with increasing $|r|$. In the Fermionic picture T_C vanishes with increasing disorder and following the BCS theory Δ becomes zero at the phase transition point, consequently ϕ becomes meaningless. In the Bosonic picture the correlator can be made vanishing at a nonzero Δ by the action of phase fluctuations of the order parameter. The next section provide a more detailed description of these theoretical models and the relevant experimental observations.

1.2 Theoretical models for the SIT

In this section the various theoretical models for the quantum phase transition[26] of the SIT, namely the Fermionic, the Bosonic and the disorder induced electrical granularity, are reviewed. It is important to note that there is no one complete theory that successfully predicts all the observed experimental results. The latter fact reflects the various system properties and the various SIT tuning parameters which ultimately result in a different physical nature of the quantum phase transition. Each theoretical model emphasizes different aspects and may fit the observed experimental results in some cases while it fails in others.

[3] Though in some cases (e.g. Al) this trend was following an opposite trend in slightly thicker films; they associated this phenomena to surface effects shifting the electron-phonon coupling to larger values due to lowering of the phonon frequencies. See ref.[12].

[4] The films were found to be amorphous and homogeneous on length scales compared to the supercodncuting coherence length by x-ray and TEM inspection.

1.2.1 Fermionic model

The effective attractive interaction between the electrons in a superconductor is the result of a competition between an attractive electron-phonon mediated interaction and a repulsive electron-electron interaction. Experimentally T_C was found to decrease with increasing disorder. Initially this change was attributed to the weakening of the electron-phonon interaction, however, later it become clear that disorder has a strong effect on the electron-electron interaction. The latter point is the essence of the Fermionic model which relies on the reduction of the density of states and the renormalization of the Coulomb or electron-electron interaction strength. Consequently, increasing disorder is predicted to reduce the value of T_C. One of the earliest theoretical work in this direction was brought forward by Maekawa and Fukuyama[27] (MF), who predicted the effect of disorder in $2D$ systems on T_C. 2D is realized when the diffusion length is restricted to $2D$, i.e. $\hbar Dq^2 > k_B T$. MF perturbation-theory yielded an expression for the reduction of T_C from the clean limit T_{C0}, written as follow:

$$ln\left(\frac{T_C}{T_{C0}}\right) = \frac{1}{2}\frac{g_1 N(0)e^2 R_{sq}}{2\pi^2\hbar}\left[ln\left(5.5\frac{\xi}{l}\frac{T_{C0}}{T_C}\right)\right]^2 - \frac{1}{3}\frac{g_1 N(0)e^2 R_{sq}}{2\pi^2\hbar}\left[ln\left(5.5\frac{\xi}{l}\frac{T_{C0}}{T_C}\right)\right]^3 \tag{1.6}$$

where R_{sq} is the resistance per square, $g_1 N(0)$ is the effective coupling constant (expected to be of the order unity), ξ_0 is the coherence length and l is the mean free path. The two terms describe the reduction of the density of states and the correction to the electron-electron interaction, respectively. Finkel'stein[28] showed that in case of $R_{sq} > 0.5k\Omega$ further corrections, beyond the MF theory, are required. He predicted the following expression for the reduction of T_C:

$$ln\left(\frac{T_C}{T_{C0}}\right) = \gamma + \frac{1}{\sqrt{2r}}ln\left(\frac{1/\gamma + r/4 - \sqrt{r/2}}{1/\gamma + r/4 + \sqrt{r/2}}\right) \tag{1.7}$$

where $\gamma = ln(\hbar/k_B\tau T_{C0})$ (τ is the scattering rate) and $r = R_{sq}e^2/(2\pi^2\hbar)$. Here the reduction of T_C due to disorder-enhanced Coulomb interactions is tuned by one fitting parameter, i.e. γ. Several experimental results, measuring the reduction of T_C as a function of disorder, exhibit good agreement with the Fermionic model, as shown in Fig. 1.1. Typical values for the fitting parameter, γ, are: 6.8 (ref.[29]) and 6.2 (ref.[30]) for TiN, 8.2 (ref.[28]) for $Mo_{79}Ge_{21}$.

1.2.2 Bosonic model

In the Bosonic model superconductivity is destroyed by phase fluctuations of the order parameter, defined in Eq.1.5. As was mentioned previously the destruction of a global phase coherent state does not necessary require that $\Delta \to 0$ all over the sample. In fact, the persistance of Cooper pairs on the insulating side of the SIT is a fundamental property of the Bosonic model, where the transition may be described by a model of interacting bosons in the presence of disorder. Here, both the Cooper pairs and the (core-less) vortices are treated as quantum mechanical objects which obey Bose statistics. Fisher et al.[31] suggested a scaling theory and later a phase diagram[32], shown in the inset of Fig. 1.2, for describing the SIT in 2D systems as a function of temperature, disorder and magnetic field[33]. In this Bosonic picture the superconducting phase is characterized by itinerant Cooper pairs and localized vortices and vice versa in the insulating phase. At the transition point both Cooper pairs and vortices are itinerant, this leads to a finite resistance. The scale of fluctuations on either side of the SIT is set by a diverging correlation length $\xi \propto \delta^{-\nu}$

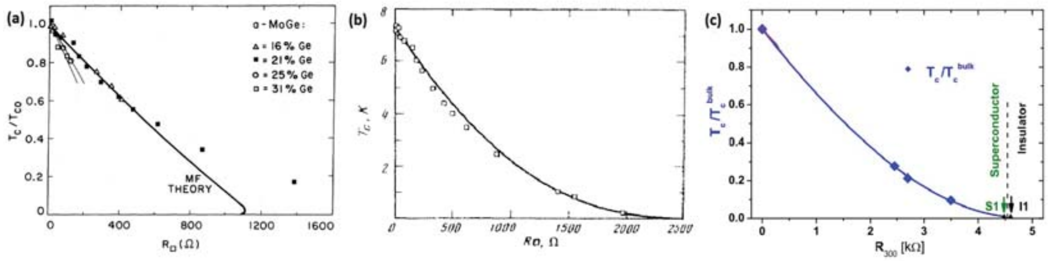

Figure 1.1: **(a),** amorphous and homogeneous thin $MoGe$ films prepared at ambient temperatures with various compositions. Figure shows the normalized critical temperature, T_C/T_{C0} versus R_{sq} for various compositions, with a fit to Maekawa and Fukuyama theory. Adopted from ref. [13]. **(b),** the same experimental results on thin $MoGo$ film with a fit to Finkel'shtein expression. Note that this fit is better than MF prediction for $R_{sq} > 0.5k\Omega$. Adopted from ref. [28]. **(c),** homogeneous TiN films deposited by atomic layer chemical vapor deposition onto a Si/SiO_2 substrates. Figure shows the reduction of T_C (blue diamonds) for several films with different nominal thickness, ranging from $3.6nm$ to $5.0nm$. The solid blue line is a fit to Finkel'shtein expression. Adopted from ref. [30].

and a vanishing characteristic frequency $\Omega \propto \xi^{-z}$. Here δ is the deviation from the critical point $\delta = |K - K_c|$, where K is the control or tuning parameter (e.g. disorder, thickness, magnetic field, etc.) which drives the system through the transition, K_c is the critical value of K at the transition, ν is the correlation length exponent and z is the dynamical critical exponent. The exponents ν and z determine the universality class of the transition. They do not depend on the microscopic details of a specific studied system, but on its dimensionality, the symmetry group of its Hamiltonian and the range of interactions between the bosonic electron pairs and vortices. The Bosonic model mentioned above predicted specific values for the critical exponents ν and z and a universal value, namely the quantum resistance of electron pairs: $h/4e^2 \sim 6.4k\Omega$, for the critical resistance at the transition point. Experimentally, a scaling analysis of the magnetic-field driven SIT on InO [17] and $MoGe$ [15] found critical exponent values which are consistent with the theory. A partial summary of experimental results from different electronic systems is shown in Fig. 1.2. The investigation of the thickness tuned transition in ultrathin films, like Bi [34] yielded similar values for the critical exponents . Moreover, in the late 80's the predicted critical value of the resistance at the transition point was experimentally observed in ultrathin amorphous Ga [35], Bi [36] and granular Sn, Pb, Ga and Al [37, 38] films as a function of thickness. The later results were performed by measurements sequences on quench condensed films, where the material is evaporated onto substrates held at low temperatures.

However, the agreement between the Bosonic model and the experimental results is far from being a general rule. Later investigation[40] of the magnetic field tuned SIT in Bi films yielded critical exponents which significantly differ from the theoretical prediction. The existence of universal critical resistance at the transition point of the SIT was also questioned. A later measurement on uniform quenched condensed Bi [41] films and thermally evaporated uniform $PbBi$ [42] films revealed a critical resistance which was significantly higher than $h/4e^2$. Similar discrepancy was also found in the case of $MoGe$ [15], while the magnetic-field tuned SIT agreed with the Bosonic theory, the critical resistance at the transition point was found to be sample dependent, as shown in Fig. 1.2. In an attempt to bridge between the latter experimental results and the Bosonic theory, a phenomenological two fluid model, i.e. normal electrons and superconducting electron

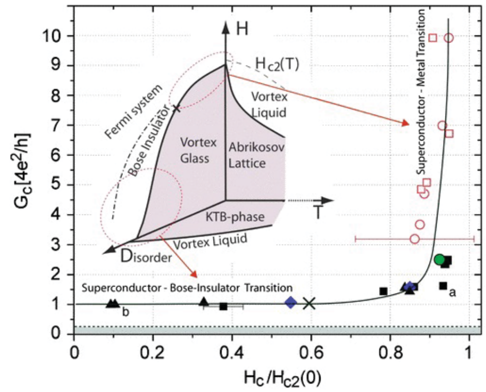

Figure 1.2: Magnetic field tuned SIT in 2D homogeneously disordered and amorphous films. The figure shows the experimentally observed critical conductance in units of the quantum conductance, $4e^2/h$, versus the critical field (defined as the point were the different isotherms of $R_{sq}(B)$ coincide) at the transition normalized by $H_{C2}(0)$ (the mean-field upper critical field at $T = 0$) in $MoGe$ (open circles and squares), Ta (full circle), InO (diamonds, full triangles and squares). The solid line is a guide to the eye. The $\times$ denotes a possible critical point between a transition to a Bose insulator and a transition to a Fermionic metal system (see ref.[39] for more details). The inset shows the generic phase diagram proposed by Fisher[32]. Adopted from ref.[39].

pairs, was considered. By estimating separately the two distinct fluids, the contribution of the Cooper pairs to the resistance at the SIT was found to be of the order of $h/4e^2$.

1.2.3 Disorder induced electrical inhomogeneity

The notion of induced electrical inhomogeneity in a scale which is larger than the underlaying disorder scale constitutes a different theoretical approach to describe the d-SIT. This idea was first brought forward as an interpretation to the measured data in a few experiments[15, 43]. Subsequently a theoretical background was constructed. In 98' Ghosal, Randeria and Trivedi[44] modeled a 2D disordered s-wave superconductor by an attractive Hubbard model with on-site disorder. Their most important conclusions were that the spectral gap in the one-particle density of states, accessible in a tunneling measurement, survives at large degrees of disorder and in a form of emerging superconducting 'islands', as seen in Fig. 1.3(a)&(b). Moreover, their numerical results suggest that even in the weak coupling case, with the superfluid stiffness[5] being much larger than the spectral gap, Δ is not spatially homogeneous in scales larger than the coherence length. Increasing disorder, however, destroys the *global* superconducting state with the demise of the long range order parameter; which follows the spectral gap in low disorder but deviates from it with increasing disorder. Being aware of Valles et al. tunneling results[41] (seen in Fig. 1.10(a)), where the spectral gap vanished with increasing disorder, they assumed that Coulomb interactions, which are not properly incorporated in their model, may cause the apparent discrepancy between theory and experiment (as mentioned previously, Coulomb interactions play a key role in the Fermionic model and are expected to have a growing effect with decreasing carrier density). With a further development in their theoretical model[46] they predicted that the spectral gap in the total

[5] The superfluid stiffness is the required energy scale to induce phase slips in the superconducting order parameter. See also ref.[45] where a special theoretical treatment is given for the evolution of this energy scale as a function of disorder

density of states not only persists in the insulating phase, but also increases with increasing disorder. Another theoretical paper which was published on the same year by Shimshoni et al.[47] delivered a similar concept of induced electrical inhomogeneity. This theory relied on the experimental results[15] on homogeneously disordered superconducting $MoGe$ that suggests a resistive response at $T = 0$. Other theoretical work[48, 49], based on Ginzburg-Landau functional and on attractive Hubbard model, reached a similar picture in which high disorder can evoke spatially inhomogeneous superconducting state in a structurally homogeneous system.

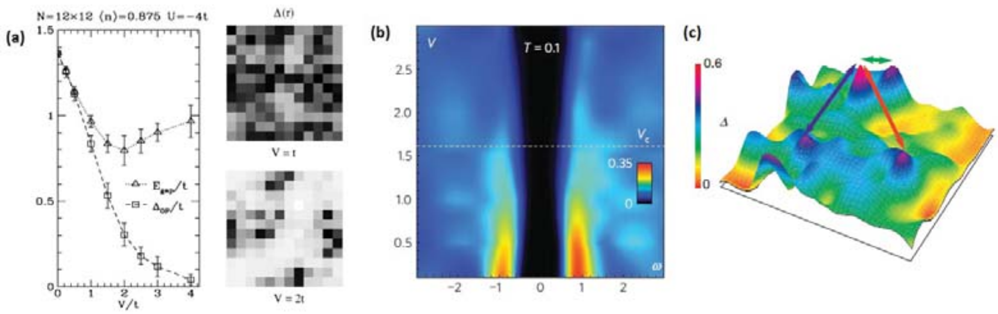

Figure 1.3: **(a),** numerical results which predict an emergent electrical inhomogeneity, employing an attractive Hubbard model with on-site disorder. Left panel: E_{gap}/t and Δ_{OP}/t versus V/t, where E_{gap} is the spectral energy gap, Δ_{OP} is defined by the spatial correlation of energy gap, V represents the degree of disorder and t is the near-neighbor hopping strength. Note that the two curves coincide for small V but gradually differ at large disorder. upper right panel: gray-scale plot showing the spatial variation of the superconducting energy gap for $V = t$ and $V = 2t$. Adopted from ref.[44]. **(b),** quantum Monte Carlo simulations which take into account both inhomogeneous amplitude variation and phase fluctuations. The figure shows the single particle density of states as a function of energy (ω) and disorder (V). Note that the superconducting gap survives across the d-SIT and its magnitude, Δ, becomes even larger deeper in the insulating side. Adopted from ref.[50]. **(c),** numerical results based on an attractive Hubbard model with disorder and a finite perpendicular magnetic field. Adopted from ref.[49].

1.3 Experimental review

In the current section the transport, tunneling and finite frequency experimental results on disorder films near the SIT are reviewed. The focus here is on homogeneously disordered thin films that undergo the d-SIT like InO, NbN and also TiN; all share several properties and experimental observations. The question whether the transition from a superconducting state to an insulating state is a direct one or via a metallic intermediate state seems to be material dependent. Varying the disorder in InO or TiN thin films never revealed such an intermediate or temperature independent resistance state while crossing the d-SIT[6]. On the other hand, in some materials a normal metal state is clearly observed once superconductivity is destroyed, for example in amorphous thin films of Nb_xSi_{1-x} [52][7], Granular Al (see ref.[53] and references there in) and Bi [36]. Given the emergent inhomogeneous electronic nature of these films at low temperatures, as will be further elaborated through the text, comparing structurally uniform and structurally granular films is an important first step. Introducing disorder is bound to yield inhomogeneity on some length scale. Assuming that the inhomogeneous length scale exceeds the atomic spacing, it defines a characteristic granule length, d. The relevant theoretical model, uniform or granular, is primarily determined by the possibility of the generation of a superconducting state in one granule taken separately, irrespective of its environment. For this to occur, it is necessary that the average spacing between the energy levels of electrons inside the granule will be less than the superconducting gap Δ, i.e. $\delta\epsilon = (g_0 d^3)^{-1} < \Delta$, where g_0 is the density of states at the Fermi level and d^3 is the average volume of one granule. Hence, the relation $\delta\epsilon = \Delta$ determines the minimum size of an isolated granule (i.e. $d_{critical} = (g_0\Delta)^{-1/3}$). For grains smaller than this critical value the film should not be regarded as granular in our context. For grains larger than $d_{critical}$ local superconductivity is expected below the critical temperature. In the latter case there are two important energy scales, namely the charging energy (E_C) and the Josephson coupling (E_J) between the grains. E_C represents the required energy to inject an electron into the grain; increasing the grain size reduces E_C and vice versa. E_J represents the strength of the superconducting correlations between the grains; increasing the intergrain spacing reduces E_J and vice versa. Hence, the ability to form a macroscopic coherent state in a granular system depends on the intergrain spacing.

1.3.1 Transport

In 2003, Frydman[22] investigated the transport properties of granular and uniform Pb films spanning the SIT. The Pb were quenched condensed onto SiO substrate (and a thin layer of amorphous Ge), yielding a structurally granular (uniform) system. Indeed, these two types of systems lead to different $R(T)$ behaviors across the SIT. In the granular case, where each individual grain can sustain bulk properties of superconductivity, phase fluctuations between the grains can lead to an insulating $R(T)$ where the Josephson inter-granular coupling is weak. Regardless of the ground state of the granular system the $R(T)$ dramatically changes at the exact same temperature, which equals the bulk T_C of Pb films. Another interesting feature that seems to be shared by such structurally granular films is the non-monotonous (namely a local minimum, or reentrance) shape of the resistance versus temperature curves[35, 54]. Evidently, the reentrance indicates the delicate balance between two opposite phenomena. On the one hand, the formation of local superconductivity

[6] In NbN systems it is not clear whether the transition is direct or indirect, see for example the resistance versus temperature curves in ref.[51]

[7] Where the the phase transition from a superconducting state via a metallic state to an insulating state was measured as a function of decreasing Nb concentration.

and on the other hand the coupling between these local grains. In the uniform system the situation is quite different. T_C seems to decrease with decreasing thickness (or increasing disorder) until it dwindles to zero and an insulating phase emerge; indicating that the global and homogeneous superconducting order parameter gradually decays. In the insulating side of these uniform metallic films there is no immediate change in the $R(T)$ curves at some specific temperature.

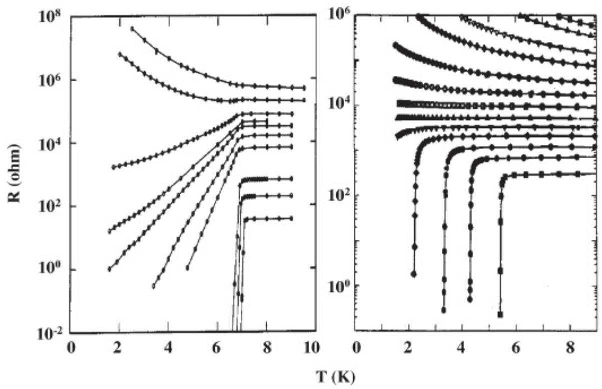

Figure 1.4: Resistance versus temperature for sequential layers of granular Pb (left panel) and uniform Pb (right panel). The different curves corresponds to different nominal thickness. Adopted from ref. [22].

Increasing disorder reduces the value of T_C; in homogeneously disordered and amorphous InO systems once T_C vanishes an insulating ground phase emerges. Fig. 1.5(a) shows the resistance per square versus temperature, $R_{sq}(T)$, curves of a few InO films spanning the SIT. Both the chemical composition (determined during the evaporation process) and the static disorder (may be reduced by annealing processes) were tuned to span the SIT. Interestingly, once the SIT is crossed into the insulating side the resistance versus temperature of the InO films follows a peculiar form. Instead of following Eq.1.1 with a stretched exponential (e.g. variable range hopping: $\nu = 1/4$, or Efros Shklovskii: $\nu = 1/2$) the $R_{sq}(T)$ follows a simple activated behavior or Arrhenius law, i.e. $\nu = 1$ so that:

$$R(T) = R_0 exp(T_0/T) \tag{1.8}$$

with a certain activation energy, T_0. With a further increase of the degree of disorder the $R_{sq}(T)$ acquires the familiar Mott variable range hopping. Fig. 1.5(b)&(c) shows the variation of T_C (in the superconducting side) and T_0 (in the insulating side) as a function of disorder across the SIT in 3D InO films. The activation energy seems to increase from $\sim 0.5K$ ($\sim 0.04meV$) up to $T_0 \sim 7K$ ($\sim 0.6meV$). In a subsequent study[43] on the 2D version of InO films the observed values of T_0 reached[8] $\sim 15K$ ($\sim 1.3meV$). The disorder here is characterize by the dimensionless parameter $k_F l$ (k_F being the Fermi wavevector and l the mean free path) obtained from room temperature resistivity and Hall effect measurements using free electron expressions[9]. However, characterizing the disorder by the parameter $k_F l$ for such disordered films (where apperently $k_F l < 1$) is a bit ill defined since l can no longer be considered as a semiclassical mean free path (acquiring values which are less than the interatomic spacing). Indeed, it was later shown experimentally[56] that by itself, $k_F l$ is not a proper parameter to define the degree of disorder. A more suitable parameter

[8] for films with similar $k_F l$ values
[9] $k_F l = [(3\pi^2)^{2/3}\hbar(R_H^{room-T})^{1/3}]/[\rho^{room-T}e^{5/3}]$ see ref. [55].

in 2D systems is the resistance per square, R_{sq}.

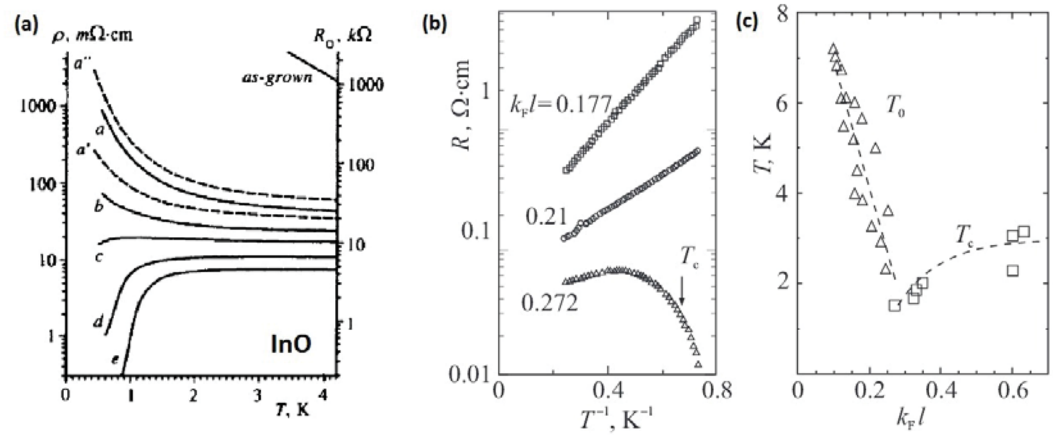

Figure 1.5: **(a),** resistivity and resistance per square, R_{sq}, versus temperature of several InO samples. Note that the value of the $R_{sq}(T)$ at the SIT point is much larger than $h/4e^2$ (as discussed in the context of the Bosonic model). Adopted from ref. [16]. **(b),** $logR$ versus $1/T(K)$ of several InO samples, the linear curves exhibit the Arrhenius or simply activated behavior of resistance; the values of the activation energy extracted from these sort of graphs are shown in panel (c). **(c),** the superconducting critical temperature, T_C, and the activation energy T_0 for InO films with a superconducting and insulating ground state, respectively. Adopted from ref. [19].

The observed simple activated behaviour of resistance versus temperature can not be reconciled with conduction mechanisms known to lead to simple activation such as nearest neighbor hopping or hopping to a mobility edge. The fact that these electronic systems are amorphous also rules out the possibility that T_0 represents the band gap of the emerging insulating phase. The physical nature of the activation energy is still in debate. A possible suggestion relying on the Bosonic or disorder induces granularity models characterize T_0 as the energy required for tunneling between superconducting islands. In 1994, Kowel and Ovadyahu [43] argued that the origin of the simply activated resistance indeed results from superconducting inclusions within an insulating matrix, as observed in structurally granular systems of macroscopic insulators which contain microscopical superconducting grains [57]. They also estimated the size of these inclusions to be in the order of $100\mathring{A} \sim 200\mathring{A}$.

This general trend of the $R_{sq}(T)$ across the SIT is not a unique property of InO. As seen in Fig. 1.6(a), TiN films with different thicknesses spanning the SIT also exhibit similar properties. The latter figure also emphasizes the negligible difference in the resistance between the "weakest" superconducting sample and the "weakest" insulating sample; in both cases it is not possible to distinguish between the two by knowing the resistance at high temperatures or even slightly above T_C. Another system that can be driven through the SIT by increasing disorder is thin NbN films. Fig. 1.6(b) shows the resistivity versus temperature for various NbN films characterized by $k_F l$ (here the values of $k_F l$ are larger than in the case of InO). The insulating phase of such NbN systems is not explored enough in the context of the current work.

All the three systems discussed in this section, namely InO, TiN and NbN, are considered homogeneous in the sense that no small structurally defined regions can sustain superconductiv-

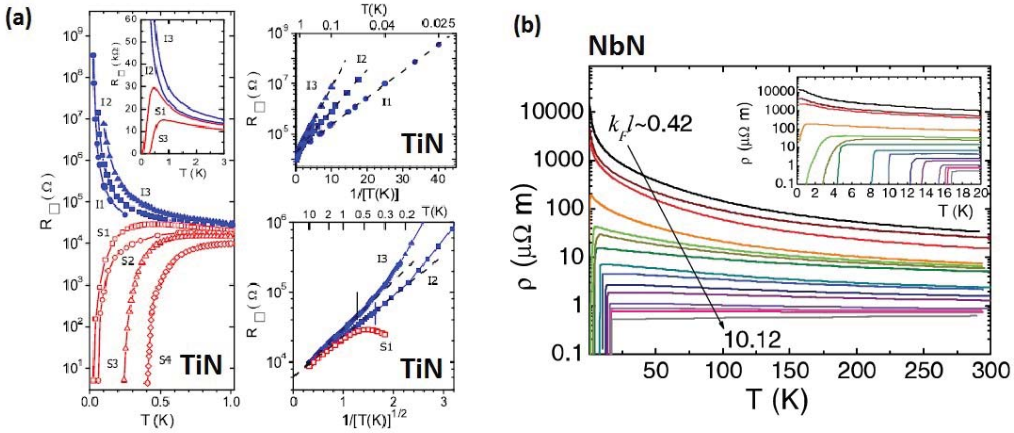

Figure 1.6: **(a),** left panel: R_{sq} versus temperature for a few TiN films spanning the d-SIT. upper right panel: $\log(R_{sq})$ versus $1/T(K)$ for three insulating samples. lower right panel: $\log(R_{sq})$ versus $1/[T(K)]^{1/2}$ for the same three insulating samples. Adopted from ref. [21]. **(b),** resistivity versus temperature for several NbN spanning the d-SIT. Adopted from ref. [20].

ity. However, as was already mentioned these films can progressively develop an inhomogeneous electronic behavior. In 2008, Kowel and Ovadyahu[58] measured the transport properties of homogeneously disorder InO samples with various lateral sizes and aspects ratios. Interestingly, the transport properties in general and the sheet resistance at the transition in particular, were found to be size dependent on mesoscopical length scales. Fig. 1.7 shows the transport behavior between differently distributed contacts deposited on top of the thin InO film. As clearly seen, the activation energy, T_0, decreases as the distance between the contacts is decreased. Moreover, as seen in the lower panel, at smaller distances between the contacts the resistance can no longer be described as simply activated. In fact the resistance seems to gradually decrease, signaling the appearance of superconductivity. In other words, over short distances the sample superconducts while over longer distances the sample behaves as an insulator. These results can be readily understood if one considers inhomogeneous electronic nature on some length scale. Hence, where the distance between the contacts approaches the inhomogeneity length scale, the $R(T)$ curves become scale dependent.

Other experimental results on InO also implies that an inhomogeneous electrical nature develops near the SIT. Current jumps were observed[59] in the current versus voltage curves on insulating InO bordering the SIT. These small jumps may indicate that the electrons transport via percolative paths between the contact electrodes. Similar results were obtained in a two dimensional array of inhomogeneously distributed quantum dots. Little-Parks oscillations were observed[60] in an insulating InO system patterned by a nanoscale periodic array of holes. The existence of superconductivity together with a macroscopic transport measurement that shows an insulating $R(T)$ behavior may also indicates the existence of isolated superconduting islands embedded in an insulating matrix. It is interesting to note that similar experimental results, were also obtained[61, 62] on Bi films[10] spanning the SIT by varying the film's thickness.

Employing magnetic field provides an important experimental knob to investigate the electronic

[10] Initially it was claimed that these Bi films, deposited on a thin Sb layer, were uniform. However, a subsequent study questioned the uniformity of these films.

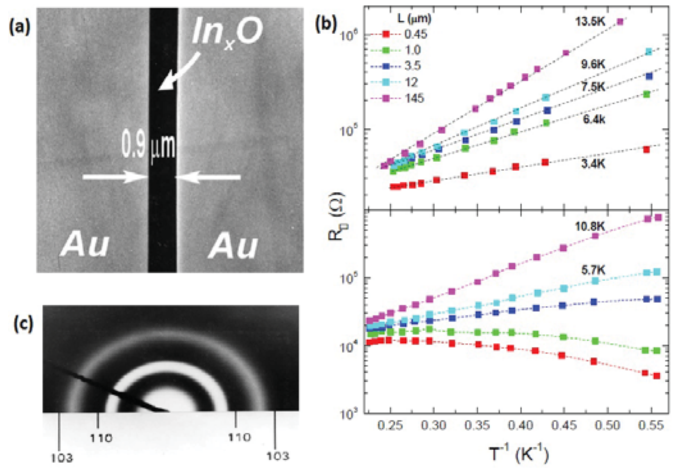

Figure 1.7: **(a),** scanning electron micrograph of a $0.9\mu m$ long amorphous InO sample. The width of the sample extends far beyonf the range shown in the image ($\sim 500\mu m$). **(b),** $logR$ versus $1/T(K)$ of an as prepared (upper panel) and thermally annealed (lower panel) InO samples with various distances between the contact electrodes. Note the gradual change in the activation energy with the distance between the contacts. **(c),** electron diffraction pattern of as prepared InO film showing only amorphous rings, in particular, the $< 110 >$ and $< 103 >$ diffraction rings of the crystalline version are not observed. Adopted from ref. [58].

nature of films. A non-monotonous magneto-resistance curve on homogeneously disordered InO and TiN[21] films has been reported by several groups. In particular, Sambandamurthy et al.[63], studied disordered InO films (prepared in a similar fashion to all InO films reported in this thesis), measured a huge magneto-resistance peak by employing parallel magnetic field. Such a behviour was not previously observed on ultrathin (quenched-condensed) films which exhibit the SIT. Dubi et al.[64] suggested a phenomenological model that relies on the assumption that disorder induces electrical granularity in these structurally homogeneous samples due to fluctuations of the superconducting order parameter amplitude[11]. The theoretical results fit perfectly to the experimental data, as seen in Fig. 1.8. The shape of the magneto-resistance curves is determined by the charging and coupling energies of the induced superconducting islands, i.e. E_C and E_j, respectively. Increasing the magnetic field from zero reduces the size of these islands, thus increasing E_C and reducing E_J; consequently results in a positive magneto-resistance. With a further increase in B-field the percolation through normal state regions becomes favorable over the percolation through these islands. At this regime the superconducting islands only hinders the conductivity, thus a further increase in B-field reduces the resistance (by reducing the average size of the islands). Dubi et al. further argued that the origin of the simple activated energy, i.e. Eq.1.1 with $\nu = 1$, is the average energy cost of Cooper pairs to percolate between the superconducting islands. It is also important to note that in structurally granular thin films, exhibiting the superconductor to insulator transition, no significant magnetoresistance is observed[12] (e.g. in Ga films mentioned above, see ref. [35]).

[11] This theoretical approach was further developed in a more rigorous manner, where the correlation between the created islands were calculated, see ref. [65].

[12] One exception to that statement is granular aluminum, where a magnetoresistance peak was observed[54] in films spanning the transition.

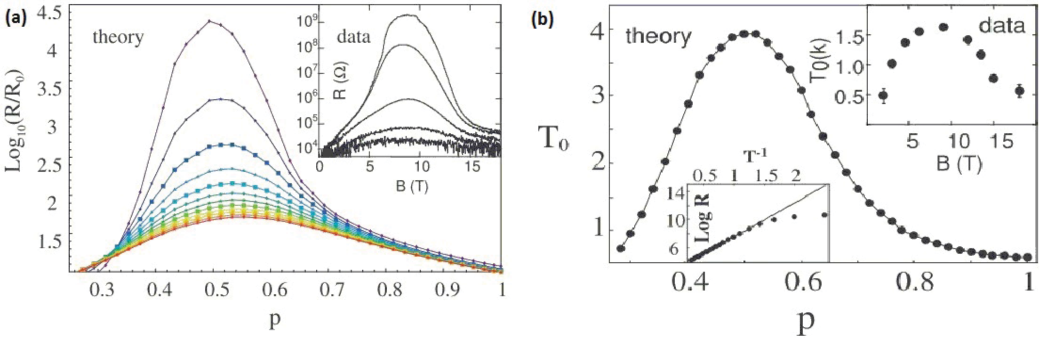

Figure 1.8: **(a),** The phenomenological model brought forward by Y. Dubi et al. [64] to describe the nature of the experimentally observed non-monotonous magneto-resistance. The thin film is modeled by a square lattice, where each site can be either normal with probability p, or superconductor, with probability $1-p$. Figure shows the numerical results as a function of probability p for different temperatures, qualitatively compared to the experimental results [63] (inset). **(b),** The activation energy T_0 obtained from the numerical calculation and from the experimental data (inset). Lower inset: an Arrhenius plot of the resistance as a function of temperature for a specific value of p. A deviation from an activated behavior is clearly seen.

1.3.2 Tunneling

Tunneling measurements provide a direct way to measure single particle density of states around the Fermi energy. The current that flows or tunnels between a normal metal through a thin insulating layer into the studied sample is proportional to the convolution of the density of states of both the normal metal and the studied sample. Assuming a constant density of states for the normal metal, the tunnel current is given by: $I(V) \sim \int_{-\infty}^{\infty} N_s[f(E) - f(E+V))]dE$, where N_s is the density of states of the studied sample and f is the Fermi distribution.

Introducing disorder in an electronic system may lead to significant effect on its density of states. The effects of electron-electron interactions in disordered electronic systems were treated adequately mainly in the two extremes, i.e. the weak and strong disorder limits. In the weak disorder limit, Altshuler and Aronov[6] found that electron-electron interactions produce a logarithmic suppression in the density of states around the Fermi energy (Eq.1.4), also known as zero bias anomaly (ZBA). The transport properties are also modified and expected to follow a lnT behavior [7]. On the other hand, in the strongly disordered regime, Efros and Shklovskii[5, 66] showed that electron-electron interactions results in stronger suppression of the density of states (Eq.1.2 & 1.3), also known as the Coulomb gap. The shape of which depends on the dimensionality. In a 2D systems the density of states is expected to be linear with energy, $G \sim |V|$. The transport properties are expected to follow Eq. 1.1 with a critical exponent equals to $\nu = 1/d + 1$.

Butko et al.[67] investigated the evolution of the tunneling density of states as a function of disorder in a uniform and amorphous (verified by electron diffraction measurements and atomic force microscopy) 2D (1.5 to 2.0nm) Be films. As seen in Fig. 1.9, at relatively low disorder the tunneling density of states follows Altshulr-Aronov expression (Eq.1.4). Increasing the disorder strengthen the depletion around the Fermi level until the expression of the strong disorder limit is observed (Eq.1.2). It is interesting to note that the least disordered sample superconducts at low temperature; in that case Δ was observed at the expected low energies, superimposed on the broad logarithmic depletions in the density of states. These experimental results were later questioned. Performing a tunneling measurement requires a metallic electrode adjacent to the studied sample (see methods section). The metallic electrode may screen the electron-electron interactions in the studied sample and consequently alter its density of states. The criticism of this work focused on an inherent problem in performing tunneling measurements to measure the effects of electron-electron interactions.

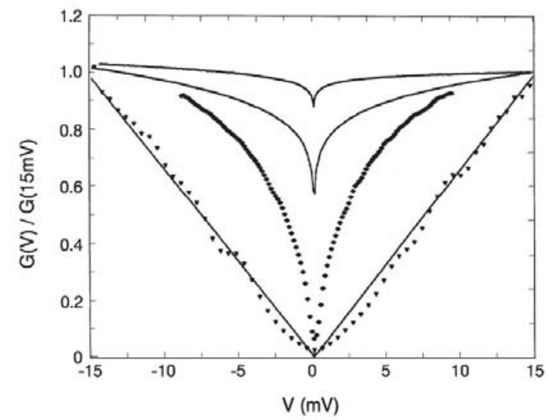

Figure 1.9: Tunnel conductance, G, normalized to $G = 15mV$ for Be films at $T = 50mK$ and resistances of $R = 530\Omega, 2600\Omega, 16000\Omega$ and $2.6M\Omega$ (top to bottom). The two least resistive samples superconducted with $T_C = 0.55K$ and $T_C = 0.33K$; in order to wipe the effect of superconductivity on the tunneling density of states a parallel magnetic field was applied. Note the gradual change from the weak disorder form of $G \sim -ln(V)$ (Altshuler-Aronov [6], also known as the zero bias anomaly(ZBA)) to high disorder $G \sim |V|$ (Efros-Shkolvskii [5, 66]). The solid lines are the best possible fits to the latter expressions. The resistance of the films was smaller than the resistance of the junctions. Adopted from ref.[67]

The emergence of a superconducting state is accompanied by the development of an energy gap, Δ, which appears in Eq.1.5, around the Fermi energy. BCS theory predicts its evolution with temperature:

$$\left(\frac{\Delta(T)}{\Delta(0)}\right) = tanh\left(\frac{T_C}{T}\frac{\Delta(T)}{\Delta(0)}\right) \tag{1.9}$$

and also predicts the following constant ratio[13] between Δ and the critical temperature: $2\Delta(T = 0)/(k_B T_C) = 3.52$. In order to extract the value of Δ from the electronic density of states, measured by tunneling spectroscopy, the following modified BCS expression is utilized:

$$N_s(E) = Re\frac{E - i\Gamma}{[(E - i\Gamma)^2 - \Delta^2]^{1/2}} \tag{1.10}$$

Where the Γ is a phenomenological broadening parameter[69], also known as Dynes parameter, resulting from finite scattering effects. In 1992, Valles et al.[41] measured the tunneling density of states of a few *uniform films* of quench condensed superconducting Bi. The structure of the planar junction geometry consisted[14] of $Al/AlO/Bi$. Fig. 1.10(a) shows the tunneling density of states of these uniform Bi films. Evidently, the superconducting order parameter, Δ, vanishes with increasing disorder. In other wards, $\Delta \to 0$ as $T_C \to 0$. Fig. 1.10(b) shows the tunneling density

[13]In the case of weak electron-phonon coupling. In the case of strong electron-coupling limit the following ratio is modified[68] and equals to ~ 4.5.

[14]The Al strip had a small amount of Mn impurities in it to prevent it from supperconduct. The Al surface was oxidiezed in ambient conditions. At low temperatures a 1-2 monolayer film of Sb was evaporated onto the surface and subsequently a series of Bi evaporations completed the junction structure.

of states of homogeneous ultrathin $PbBi/Ge$ as a function of magnetic field. Evidently, traces of superconducting energy gap persists even when the $R(T)$ curves exhibit a negative dR/dT. This result is consistent with the Bosonic picture; however at the d-SIT in this material the critical sheet resistance is above the Bosonic theory expectation value (i.e. $R = 8K\Omega > h/4e^2$).

On the other hand, in structurally *granular films* the situation is quite different. Measuring[69] the tunneling density of states of granular quench condensed Sn films on a similar junction geometry (i.e. $Al/Al0/Sn$) yielded roughly the same value of Δ for films with various sheet resistance, ranging from $R_{sq} = 542\Omega$ to $\sim 10k\Omega$. The difference between the tunneling curves was only reflected in the broadening parameter, Γ. In fact, several years later, employing an $Al(Mn-doped)/AlO/Pb$ planar junction arrangement, it was experimentally shown[70] that the value of the superconducting energy gap remains constant through the SIT. Fig. 1.10(c) shows the tunneling current as a function of voltage for both superconducting and insulating films, evidently the curves are very similar. Examining the temperature evolution of Δ in the insulating sample yielded good agreement with the BCS prediction, as seen in Fig. 1.10(d).

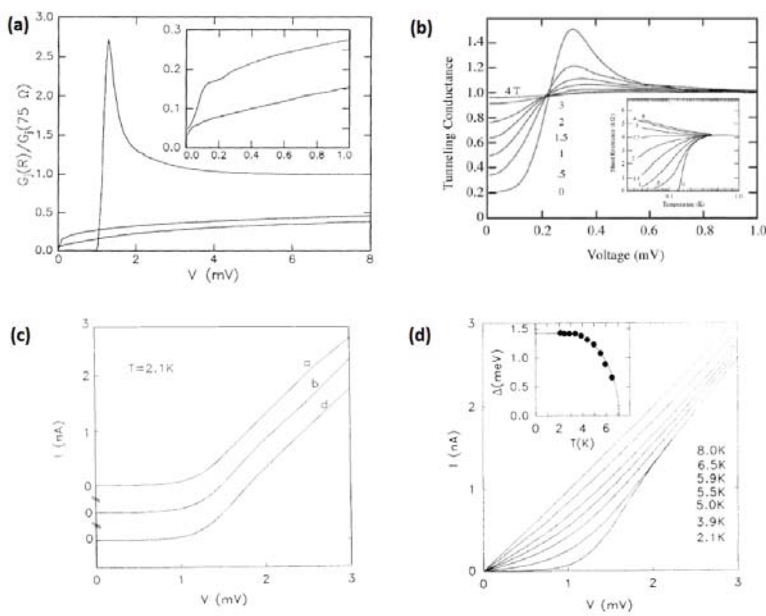

Figure 1.10: **(a),** tunneling conductance versus junction voltage of thin uniform Bi films with $R_{sq} = 8.0k\Omega$ (lowest curve), $R_{sq} = 5.8k\Omega$ (middle curve) and $R_{sq} = 0.075k\Omega$ (upper curve). Inset: the two resistive films on an extended scale. Note that Δ seems to vanish with increasing disorder. Adopted from ref.[41]. **(b),** Tunneling density of states versus junction voltage of thin uniform $PbBi$ films at several magnetic field strengths. Inset: the corresponding resistance versus temperature curves. Note that Δ seems to persists even at magnetic fields which results in non superconducting $R(T)$ trends. Adopted from ref [42]. **(c),** current versus voltage characteristics of superconducting (b and d) and insulating (a) granular Pb films. Note that there is hardly any difference between the curves; indicating the Δ remains constant through the SIT in granular metallic films. Adopted from ref.[70]. **(d),** similar plot but only for the insulating film. the different curves corresponds to different temperatures, ranging from $2.1K$ to $6.5K$. Inset: $\Delta(T)$ obtained from a fit to the BCS expression of Eq.1.10. Note the remarkable agreement with the theoretical curve for Pb. Adopted from ref.[70].

In conclusion, as T_C is decreased with increasing disorder (decreasing thickness) $\Delta \to 0$ in uniform metals and $\Delta \to const$ in granular metals.

Next we turn to *homogeneously disorder films*, such as InO, TiN and NbN. The tunneling density of states shares some peculiar properties between these films. Fig. 1.11 shows local scanning tunneling microscopy (STM) on TiN and NbN thin films. Clearly the superconducting order parameter is not uniformly distributed across the sample. The observed variation in Δ is not correlated with the structural features. The similarity between these results and the numerical results shown in Fig. 1.3 is evident. It may be important to note that such an emergent electrical inhomogeneity was also observed[25] by local STM measurements in low-carrier density version of high-Tc superconductors.

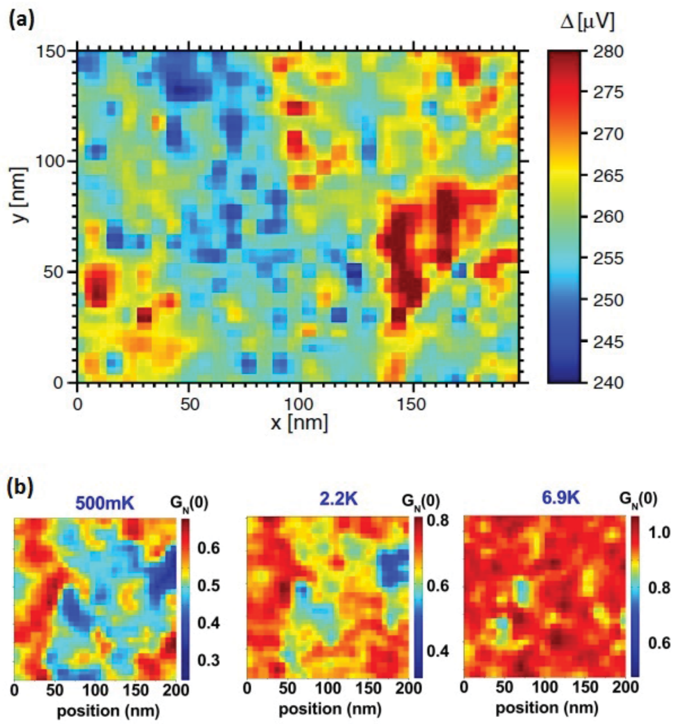

Figure 1.11: **(a),** Local-STM measurement shows spatial fluctuations of Δ on a thin (4 6nm) TiN film with $T_C = 1.3K$. The observed spatial features do not corresponds to any structural features. Note the similarity to the numerical simulations shown in Fig. 1.3, however, as seen in the scale of Δ the value of Δ varies by less than 20%. Adopted from ref.[30]. **(b),** temperature evolution of emergent inhomogeneity, observed by a local-STM, in a thin NbN film with $T_C = 2.9K$. The observed spatial features do not corresponds to any structural features. Adopted from ref.[71].

The superconducting gap is expected to vanish at the critical temperature. Indeed in normal metal superconductors, $\Delta \to 0$ where $T \to T_C$. Hence, the appearance of Δ signals the emerging superconducting state. Indeed, in the standard BCS theory, Cooper pairs are energetically advantageous at $T < T_C$ and the range of temperatures in which fluctuations in the order parameter are significant is extremely narrow. However, in high-Tc superconductors it was discovered that a noticeable suppression, similar in magnitude to Δ (below T_C) in the density of states emerges above T_C, this feature is known as a pseudogap. Recently, such a pseudogap was observed in homogeneously disorder films of InO, TiN and NbN, as seen in Fig. 1.12. Being conventional or s-wave superconductors these latter experimental results are intriguing.

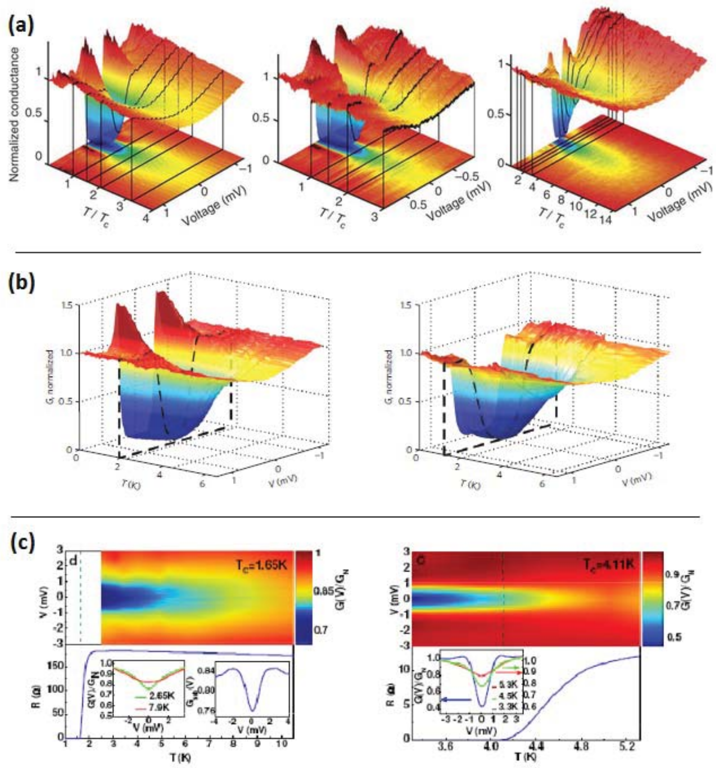

Figure 1.12: Pseudo gap observed in tunneling measurements. **(a),** 3D plots of the tunneling conductance normalized by the conductance at high voltage as a function oof junction voltage and normalized temperature, T/T_C for three superconducting TiN films. The films differ in their disorder an T_C which range between $\sim 0.3K$ to $\sim 1.25K$, corresponding to right, middle and left figures, respectively. Note that the pseudogap is more pronounced and persists to higher temperatures as the disorder is increased. Adopted from ref.[72]. **(b),** similar measurement but on superconducting InO samples with relatively low disorder (left panel) and high disorder (right panel). Note that psedugap is similar between these two films. However, the coherence peaks at the edges of the superconducting gap in the high disorder sample are absent, unlike the low disorder sample.. Adopted from ref.[73]. **(c),** local-STM measurement of the density of states of NbN films with $T_C = 1.65K$ (left panel, the corresponding $R(T)$ curve is shown in the bottom) and $T_C = 4.11K$ (right panel, the corresponding $R(T)$ curve is shown in the bottom). Adopted from ref.[20].

1.3.3 Finite frequency measurements

The use of finite frequency measurements may provide more details on a studied physical system than dc measurement. Most importantly, ac probing as opposed to dc probing, allows to extract the complex response function of the electronic system, i.e. both the real and the imaginary part of the various response functions[15]; for example the complex conductivity, $\sigma_1 + i\sigma_2$, the complex dielectric function, $\epsilon_1 + i\epsilon_2$, or the complex sheet impedance of a thin film $1/\sigma d = R + i\omega L$. The real part of the conductivity, which is the in-phase response, reveals information about the dissipation in the system while the imaginary part of the conductivity, which is the out-of-phase response, reveals the polarization of the charge carriers and their ability to move without dissipation. A few particular advantages of ac over dc probing are that the former technique enables to detect both the superconducting gap, Δ, and the superfluid stiffness, D_s. The latter parameter describes the phase rigidity of the superconducting order parameter and it is directly linked to the imaginary part of the conductivity: $\sigma_2 = \frac{4e^2}{\hbar d} \frac{k_B D_s}{\hbar\omega}$. However, this relation between the measured σ_2 and D_s is valid for probing energies which are bellow the pair breaking energy[16]: $\hbar\omega < 2\Delta$. Another important advantage of ac measurements is the fact that it is less (or completely not) sensitive to percolation paths, as opposed to dc measurements. Hence it may characterize true average bulk values without being controlled by specific small areas which may effect the observed results. Despite their potential impact there have been very few experiments utilizing finite frequency measurements in the vicinity of the SIT. This is largely due to the required technical conditions like frequencies above solid state systems (network analyzers reach a few tens of Gigahertz, $\sim 0.1meV$) but below infrared and low temperatures (while still employing optical cryostat in the case of free space spectroscopy) which pose significant challenges.

Recently the response function of homogeneously disorder InO samples was probed in the microwave regime by means of cavity resonator[75] and Corbino arrangement at zero H-field[76] and as a function of perpendicular H-fields[77]. In these measurements there is no need to employ an optical cryostat, since the radiation does not transverse in free-space, thus lower temperatures are more easily accessible. In principle, at these low frequencies relatively to 2Δ, σ_1 is expected to remain negligible while σ_2 rapidly increases as $1/\omega$. Hence the superfluid stiffness, being proportional to $\omega\sigma_2$, can be directly extracted. Fig. 1.13 shows that the superfluid stiffness survives well into the insulating regime and also at $H > H_C$, where H_C is the critical magnetic field. It is important to note that the existence of superfluid stiffness at finite frequency at $H > H_C$ is not inconsistent with an insulating ground state. That is since finite frequency measurements are sensitive to superfluid fluctuations due to the short time scales of the microwave radiation; probing below a certain order parameter fluctuation rate will not be sensitive to such fluctuations and the observed D_s is expected to vanish. At low temperatures and well into the insulating side the superfluid stiffness becomes temperature independent as $T \to 0$. This shows that the observed effects are not thermally driven and is indicative of their intrinsic quantum mechanical nature. These results shows unambiguously that at some region above the critical H-field the insulating state is dominated by superconducting correlations, hence it is consistent with the Bosonic picture. However, it can not rule out the idea of disorder induced inhomogeneity discussed earlier.

A microwave measurement, utilizing Corbino arrangement, on NbN films revealed similar re-

[15] All these response functions are linked via simple electrodynamics expression. Moreover, the imaginary and the real part of a particular response function are linked via Kramers-Kronig relation. See ref.[74] for detailed expression.

[16] see review in chapter 3 of "introduction to superconductivity" 2nd edition, Dover Publishing, by M.Tinkham.

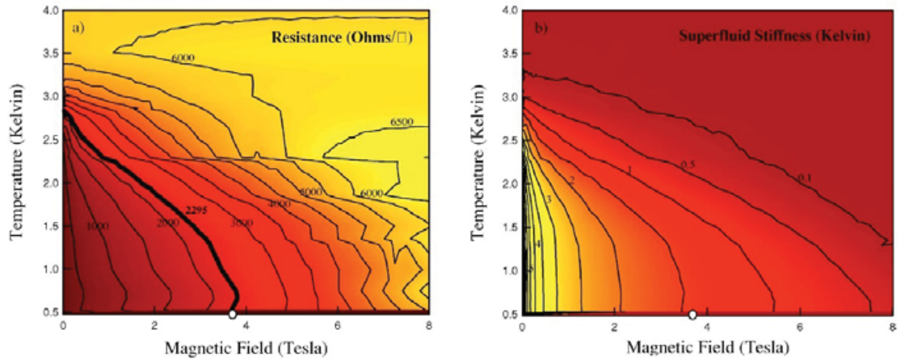

Figure 1.13: **(a),** ac sheet resistance, $\propto Re(1/\sigma d)$ versus temperature and magnetic field. The bold line is the critical resistance extrapolated to finite temperature. **(b),** superfluid stiffness ($\propto \omega\sigma_2$) at $22GHz$. The critical field H_{SIT} is shown as a white dot at $H = 3.68T$. Yellow indicates maximum. Adopted from ref.[75].

sults. Fig.1.14 shows the complex conductivity ($\sigma_1 + i\sigma_2$) of an homogeneously disorder NbN films close[17] to the d-SIT. Clearly the superconducting critical temperature is not marking any dramatic change in the observed σ_1 and σ_2 curves. Interestingly, it seems that a minimum is developed with decreasing temperature in σ_1 at $f \sim 12GHz$. According to the extension of the BCS theory to finite frequency, brought forward by Mattis and Bardeen[78], the minimum in σ_1 marks the value of 2Δ. Hence it appears that the superconducting gap is surprisingly observed at these low frequencies; while according to tunneling measurements on similar samples the minimum in σ_1 should have been observed at about an order of magnitude higher frequency. Our interpretation of these results is given in chapter 3.4 "Higgs mode near the d-SIT".

Detecting the actual value of the superconducting gap, Δ, with a finite frequency measurement requires a photon energy in the Terahertz (THz) spectrum, which is higher than microwave and lower than infrared. THz spectroscopy is a well established and common method to detect superconducting correlations and in particularly to detect Δ. In general, the response of ordinary metallic s-wave superconductors is successfully characterized by Mattis-Bardeen[78] expression. Table 1.3.3 briefly summarizes several THz spectroscopy measurements on s-wave superconductors and describes the various quantities that may be extracted directly and indirectly from such measurements.

[17]The critical temperature of the cleanest NbN sample is $\sim 15.5K$, while for the sample shown here $T_C \sim 3.14K$.

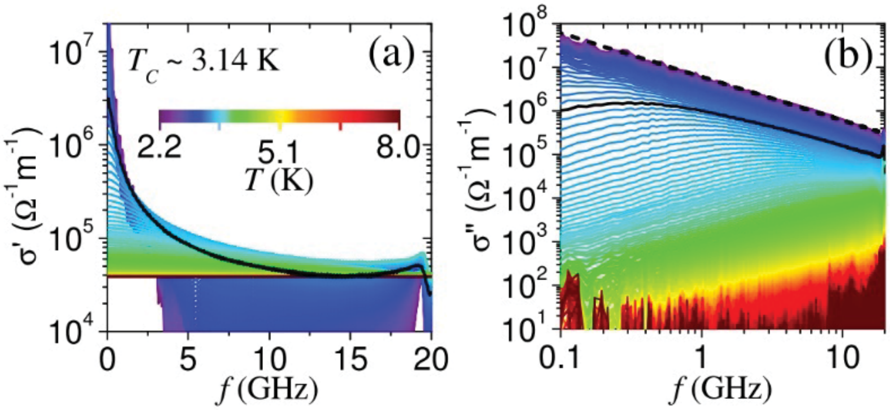

Figure 1.14: The complex conductivity of a highly disorder superconducting NbN sample with $T_C \sim 3.14K$, measured in the microwave regime utilizing a Corbino setup. **(a),** the real part of the complex conductivity, σ' versus frequency. Note the minimum that develops around $f \sim 12GHz$ with decreasing temperature. The dramatic increase observed toward $f \to 0$ is due to the broadening of the σ_{dc} due to finite temperature effects. **(b),** the imaginary part of the complex conductivity on a log-log scale. Note that the superfluid stiffness, D_s, persists to temperatures above T_C. Adopted from ref.[79].

Material	T_C	$2\Delta(0)$	$2\Delta(0)/k_BT_C$	$\lambda(0)$	ξ_0	n_S	ref.
$NbTiN$	$14.1K$	$36.5cm^{-1}$	3.72	$260nm$	$170nm$	N/A	[80]
$Nb_{1-x}Ti_xN$	$8.5K$	$24cm^{-1}$	4	N/A	N/A	N/A	[81]
NbN	$15.4K$	$\sim 50cm^{-1}$	~ 4.6	N/A	N/A	N/A	[82]
NbN	$15.1K$	$43.3cm^{-1}$	4.12	N/A	N/A	N/A	[83]
NbN	$8.31K$	$24cm^{-1}$	4.1	$90nm$	$39nm$	$l = 9nm$ @T=9K	[84]
$\alpha - MoGe$	$4.5K$	-	3.7	N/A	N/A	$1.210^{21}cm^{-3}$	[85]
$\alpha - MoGe$	$6.9K$	-	3.8	N/A	N/A	$1.610^{21}cm^{-3}$	[85]
TiN	$3.4K$	$8.14cm^{-1}$	3.44	$\sim 730nm$	x	$1.610^{21}cm^{-3}$	[86]
$MgBi$	$6.9K$	-	3.8	N/A	N/A	$1.610^{21}cm^{-3}$	[87]
TaN	$9.7K$	-	3.3	$\sim 500nm$	N/A	N/A	[88]
TaN	$8.5K$	-	3.6	$\sim 500nm$	N/A	N/A	[88]

Table 1.1: Summary of THz optical spectroscopy results on several s-wave superconductors. The following expression was used to obtained the coherence length: $\xi_0 = \hbar v_F/\pi\Delta(0)$. In the case of $NbTiN$ the estimated value of Fermi velocity was: $v_F = 1.9 \times 10^6 m/s$. Here the film is in the so called dirty-limit, i.e. $l << \xi_0$, and in the local regime, i.e. $\xi < \lambda(0)$ (see ref.[74, 89] for details about the various regimes). For the TiN case the London penetration depth, $\lambda(0)$, was obtained by using the two-fluid model with $\lambda_L^2(0)/\lambda_L^2(T) = 1 - (T/T_C)^4$. Where $\lambda_L = \sqrt{c^2/4\pi\omega\sigma_2}$.

Chapter 2

Materials and methods

2.1 Materials

2.1.1 Indium Oxide

Our primary system of choice for this study is amorphous and homogeneously disorder indium oxide samples. The films were deposited by e-gun evaporation[1] while dry and pure (99.999%) oxygen was injected into the chamber at a certain partial pressure which ultimately determines the electron carrier density and subsequently the ground state of the sample. For a partial oxygen pressure in the range of 0.5 to $\sim 5 \times 10^{-4}$ Torr, the sample ground state is an insulator with a low carrier density in the range of $(0.1 - 10) \times 10^{19} cm^{-3}$. For a partial oxygen pressure of ~ 0.5 to 5×10^{-5} Torr, the sample ground state is a superconductor with a carrier density that can reach $\sim 10^{21} cm^{-3}$ (for discussion about the experimental extraction of carrier density see ref.[56] and references therein). The SIT can also be spanned by annealing in vacuum at $T \sim 50C$, which is below the crystallization temperature, $\sim 150C$. The latter process reduces the static disorder in the film and consequently the resistance is reduced; the carrier density, however, remains constant. It is important to note that in order to span the SIT by sequences of annealing processes a minimal required electron carrier density must be met. The methods describe here is identical to previous works on InO reported in the introduction chapter, e.g.[19, 43, 56, 58, 59, 73, 90]. We used atomic force microscopy to measure the surface roughness, as shown in Fig.2.1(a), and found that the typical height variation has a root mean square of a few nanometers (similar to previous work on InO). Electron diffraction patterns, shown in Fig.2.1(b) revealed[56] the absence of any diffraction ring of either crystalline indium oxide or metallic indium. The dimensionality of these films depends on several parameters like the mean free path l, the superconducting coherence length ξ, the Fermi wave length λ_F and the thermal length l_T. For low voltage and temperature in the normal state a typical film's thickness of $30nm$ is smaller than l_T, thus the theoretical treatment should be of a 2D system. In the superconducting state, films with such thickness are of the same order of ξ, thus they should be treated as quasi-2D systems.

Recently Givan and Ovadyahu[56] presented transport and scanning transmission electron microscopy (STEM) results on several indium oxide samples with a various degree of electron concentration. Fig. 2.2(a)&(b) show STEM images for low and high carrier density versions of amorphous

[1] There are other methods to deposit thin indium oxide films, however they may, and usually are, result in a different chemical and structural characteristics.

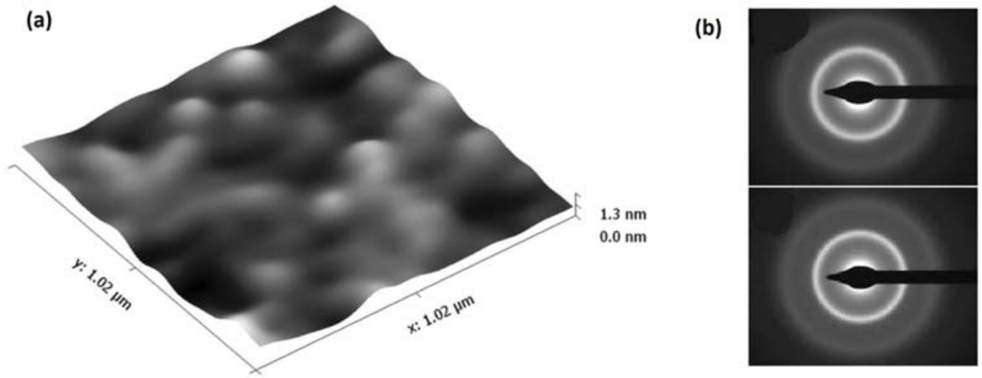

Figure 2.1: **(a),** an AFM image of a $30nm$ thick InO film. The RMS of the surface roughness is $1.5nm$. This result is typical for such InO films, regardless to the partial oxide pressure during the evaporation. **(b),** electron diffraction patterns of as prepared (upper panel) and same sample after thermal annealing for 34 days (lower panel). The as-deposited sample had an $R_{sq}^{T=300K} \sim 120M\Omega$ and the after annealing $R_{sq}^{T=300K} = 70k\Omega$. Note that in both cases the electron diffraction pattern is practically identical and exhibiting that the film is amorphous. Adopted from ref.[56].

indium oxide thin films, yielding insulating and superconducting ground states, respectively. The most important finding is the spatial fluctuations of the carrier concentration[2], persisting over scales of up to $300 - 800$Å, as can be seen in Fig. 2.2(c) which show the Fourier transform of the STEM image. These scales are in the order of the length scales relevant for transport in general and the superconducting coherence length in particular. This demonstrates that the scenario of disorder induced inhomogeneity should be considered in any theoretical attempt to describe the physical nature of such disorder films, particularly at low temperatures and close to the d-SIT. Another important observation, brought forward by Givan and Ovadyahu, is that $k_F l$ is not a good parameter to characterize disorder when superconductivity is present. In fact, they showed that reducing k_F by decreasing the carrier density (increasing the partial oxide pressure during the film's evaporation) reduces the value of T_C more than reducing l (increasing the static disorder), even when the value of $k_F l$ is kept unchanged.

2.1.2 Niobium Nitride

The NbN films we have measured in our THz spectroscopy system were grown by our Colleagues in Mumbai, namely Pratap Raychaudhuri and John Jesudasan. The films were synthesized through reactive dc magnetron sputtering by sputtering a Nb target in an $Ar - N_2$ gas mixture. The substrate temperature and ambient pressure during growth for all the films were fixed at $600C$ and $5mTorr$, respectively. The carrier density is varied by changing the ratio of N_2 and Ar. Ref. [92] gives a description of the properties of these NbN films with relatively low disorder; i.e. between films with $T_C \sim 10K$ (and $\rho \sim 3.83\mu\Omega m$) and $T_C \sim 16.1K$ (and $\rho \sim 0.94\mu\Omega m$). Using Hall effect measurements the following carrier density were found in the corresponding films: $n \sim 6.47 \times 10^{22} cm^3$ and $n \sim 1.98 \times 10^{23} cm^3$; employing free electron expression (see section 1.2.1) they derived the following $k_F l$ values: $k_F l \sim 2.56$ and $k_F l \sim 7.15$. NbN films with higher degree of disorder and closer to the quantum phase transition are discussed in ref.[20]. For such highly

[2]Interestingly, similar conclusions were lately derived[91] for a disordered 2D electronic system of graphene

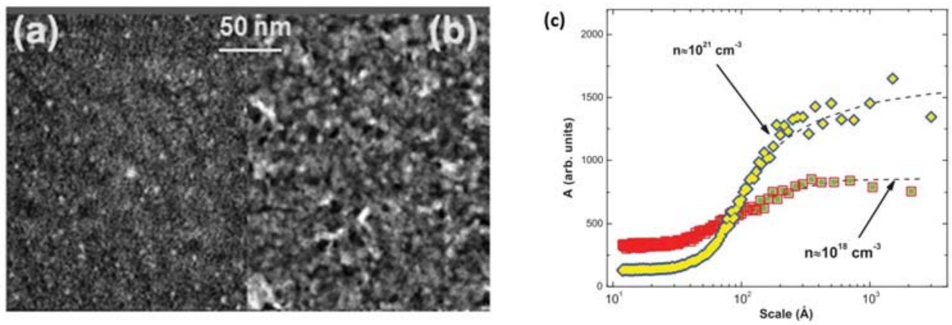

Figure 2.2: **(a),(b)**, a scanning image of a transmission electron microscope of low (a) and high (b) carrier density InO films, $5 \times 10^{18} cm^{-3}$ and $3 \times 10^{21} cm^{-3}$, respectively. The contrast mechanism in the micrograph is due to absorption. The bright colors signify oxygen rich patches and vice versa for the black colors. Adopted from ref.[56]. **(c)**, Fourier transform of the STEM image. These were averaged over individual line scans taken across each micrograph. The dashed lines are merely guides to the eye. Adopted from ref.[56].

disordered films T_C was observed to decrease below $0.3K$ (their lowest available temperature). With increasing disorder, practically achieved by reducing the carrier density, the dimensionless parameter $k_F l$ was further decreased. For samples with $k_F l < 1$ no superconducting behavior was observed down to $300mK$.

2.2 Methods

2.2.1 Tunneling and transport

We have used both He-3 and Dilution refrigerator systems in our transport and tunneling measurements. The *transport* measurements, relevant in all our work, were performed by 2 or 4 contacts utilizing standard Kiethley 2400 or Yokogawa 7651 dc sources and Kiethley 2000 voltmeters (see Fig.2.3(a)). Special care was taken to ensure the persistence of an Ohmic response, especially in the insulators, usually by reducing the driving current below $0.1\mu A$. However, while measuring very high resistances, we utilized a Femto DDCPA-300 current amplifier. This current amplifier serves as a virtual grounding. Hence for measuring a highly resistive sample a two-contact arrangement is preferable; one end connected to a dc voltage source and the other end to the input of the current amplifier. The output of the current amplifier is held at a dc voltage equal to the input current multiplied by a chosen factor between 10^4 to 10^{13}. Practically, low-frequency noises (e.g. $50Hz$ from various sources) will also be multiplied, consequently saturating the output voltage before reaching the maximum amplification. Hence, in order to maximize the current amplification, special care was taken to reduce low frequency noises by using low pass filters and clean grounding.

The *tunneling* measurements, as described in paper 6.1, were based on a planar tunneling junction (see Fig.2.3(b)). A $30nm$ Al stripe was thermally evaporated (at a rate of $\sim 0.5A/s$) on a Si/SiO substrate and was allowed to oxidize for a few hours in ambient conditions with slightly more humidity (which helps to form a more resistive AlO surface, reaching as high as $1M\Omega$). Subsequently, a $31nm$ InO stripe was e-gun evaporated perpendicular to the Al/AlO stripe, thus forming a planar tunnel junction with barrier dimensions of $1 \times 1mm$. To obtain the tunneling density of state we have directly measured the dI/dV in the following way: a small step function dc voltage sweep was connected to one end of the Al strip and the current amplifier was connected to the InO strip. Parallel to the dc sweep a Lock-in amplifier (Stanford SR830 or EG&G 7265) was employed to inject and read a small ac ($\sim 10Hz$) on the same contacts (i.e. between the Al and the InO strips). The latter measurements is basically the derivative of the $I - V$ characteristic, thus it is proportional to the density of states of the InO sample (assuming the density of states of the Al is constant). Special care was given to verify that the tunnel barrier resistance was at least an order of magnitude larger than the InO resistance (otherwise the measured signal will represent characteristic of the InO stripe instead of junction barrier).

2.2.2 THz spectroscopy

In the past two decades a significant progress in the field of Terahertz spectroscopy brought forward new opportunities to optically probe energies in the vicinity of the superconducting energy gap. Although being used intensively in many research fields it is still absent in the field of disordered superconductors. Using this tool to probe disordered conventional s-wave superconductors, in particular close to the d-SIT, poses many technical challenges. In the first place, it requires low temperatures while employing an optical cryostat, allowing the THz radiation to pass through the cryostat and the sample with minimal intensity reduction. In the second place, using radiation in the sub millimeter wave length generates many standing waves and parasitic radiation; usually this is the major obstacle (see the discussion the technical review, ref.[88]). The two prime methods to detect the complex response function of a system in the Terahertz regime are time-domain and frequency-domian spectroscopy. In the time-domain method a fast radiation pulse is emitted on the studied sample and the THz spectrum is recovered by using Fourier transform. In the frequency domain method a coherent radiation source is utilized to independently measure each frequency per temperature. We used the latter method, employing a system in Martin Dressel's lab at the university of Stuttgart. The system was arranged as a free-space Mach-Zehnder interferometer, sketched in Fig.2.4(a), to measure two optical quantities: the transmission through the sample and the phase shift caused by the sample. Each of these measurements is compared to an empty sample holder in order to compensate for radiation intensity variation and physical changes in the submillimeter scale at one or more points in the system. An example of "raw" data, i.e. transmission and phase shift, of a clean NbN sample is shown in Fig. 2.5(a). Both of these optical parameters are directly linked to the complex response function of the sample via Fresnel equations (see Eq.1 in paper 6.3). The coherent radiation source employed here is a backward wave oscillator (BWO), which essentially hosts different resonators; each tuned to a small bandwidth in the THz range (defined here as $0.05 - 1.2THz$, corresponding to a photon energy of $0.18 - 5meV$) and each produce different photon intensity, as seen in Fig.2.4(b). The photon intensity is important in determining the sensitivity of the system, which is especially relevant for disorder films with low conductivity and subsequently almost transparent (see Fig.2.5(b).).

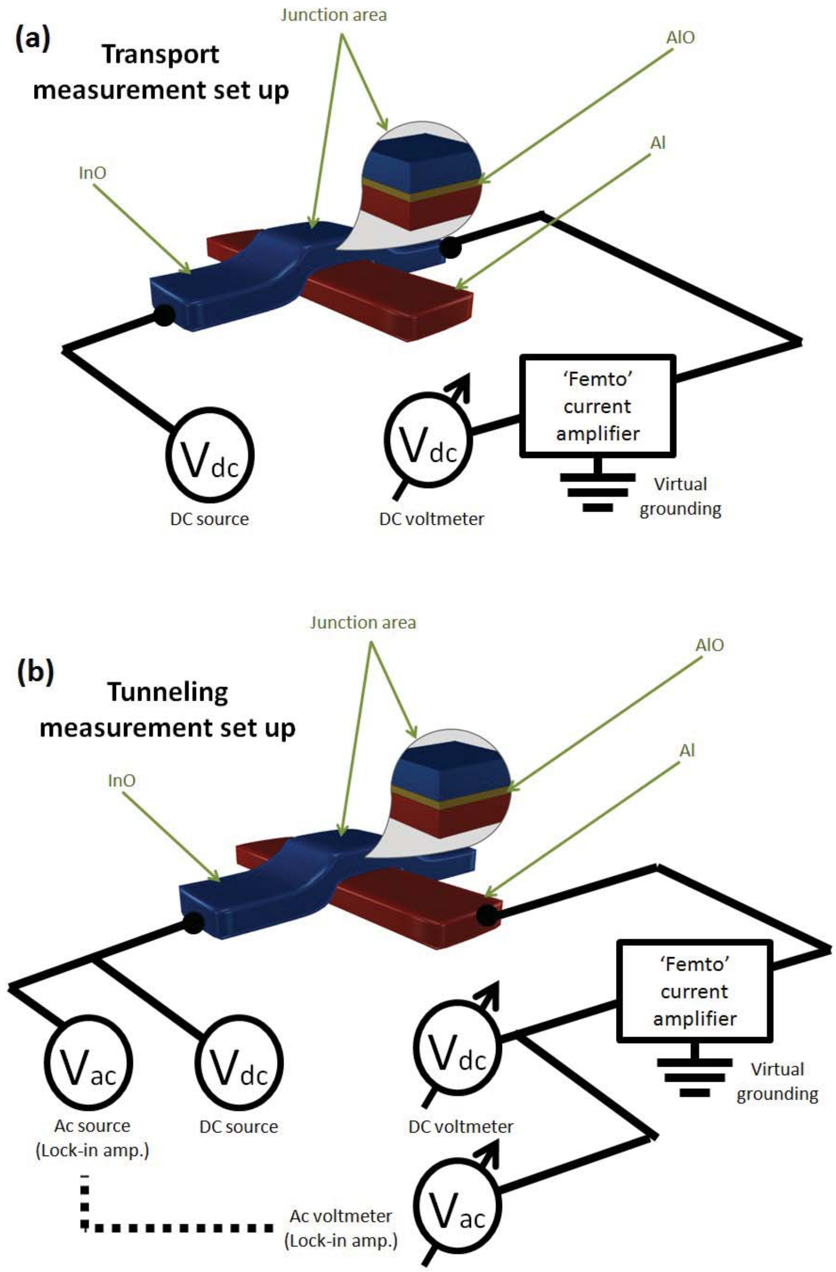

Figure 2.3: Simplified sketch of the transport (a) and tunneling (b) measurement setups. Note that in the transport setup the entire sample is probed whereas in the tunneling setup only part (effectively only the region above the junction are) of the sample is probed. In the tunneling setup the dc and ac sources are connected to the sample via a voltage divider. The dc source sweeps the energy across the junction and the small ac signal enables to directly measure the derivative: dI/dV. The density of state is extracted from the latter curve, see section 1.2.2.

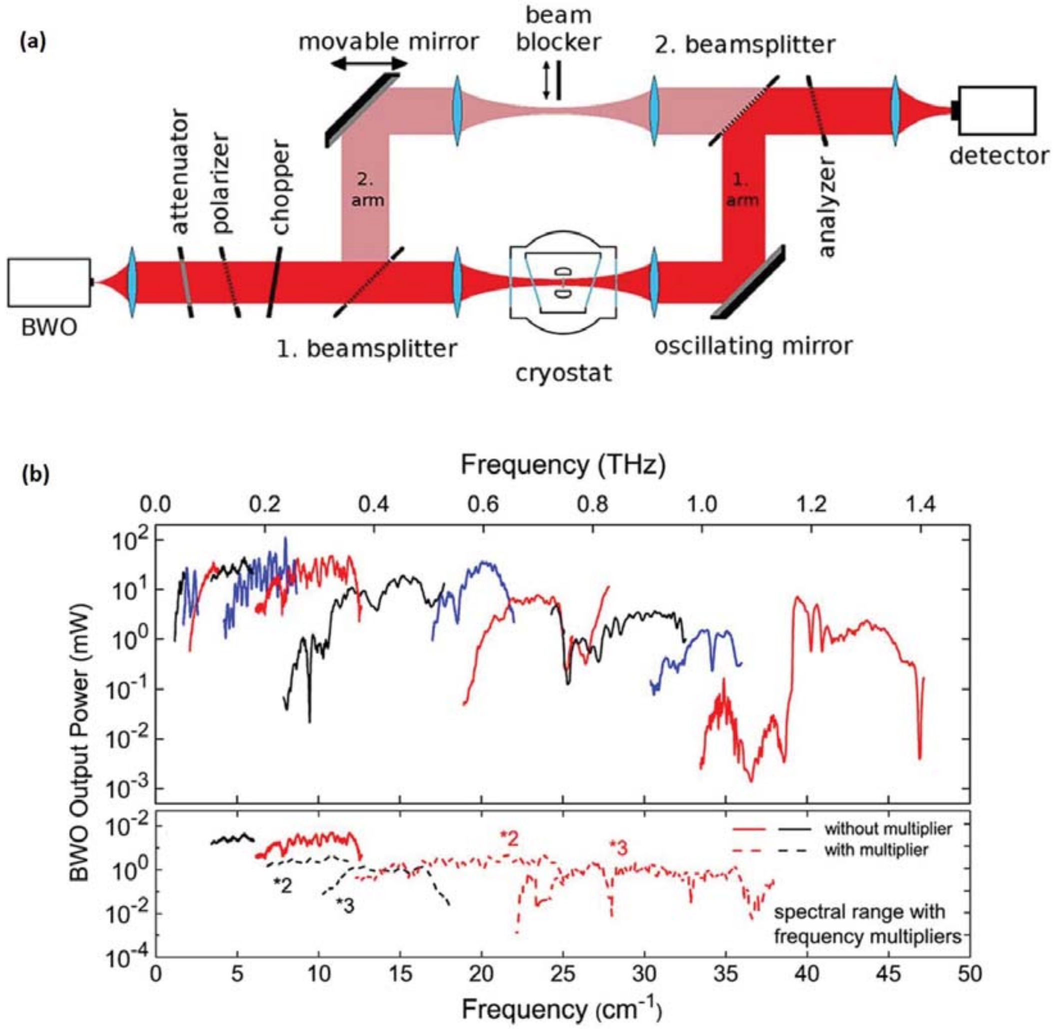

Figure 2.4: **(a),** simplified sketch of the THz measurement setup. The system is arranged as a Mach-Zehnder interferometer, employing two distinct arms. The strong red colored arm (Arm 1) is used to measure the transmission through the studied sample. Both arms are used to measure the phase shift of the radiation transversing through the sample. The source of the coherent THz radiation is a BWO and the detector is a Golay cell. Adopted from ref.[88]. **(b),** upper panel: the output power of the various BWO sources versus frequency. The range from 1 to $47cm^{-1}$ is completely covered. Lower panel: the available spectral range of a source can be increased using passive frequency doubler and tripler (dashed lines). The signal intensity in the doubled/tripled spectral range, however, is 3 to 4 orders of magnitude smaller and usually require the use of a ^4He-cooled bolometer for detection. Adopted from ref.[88].

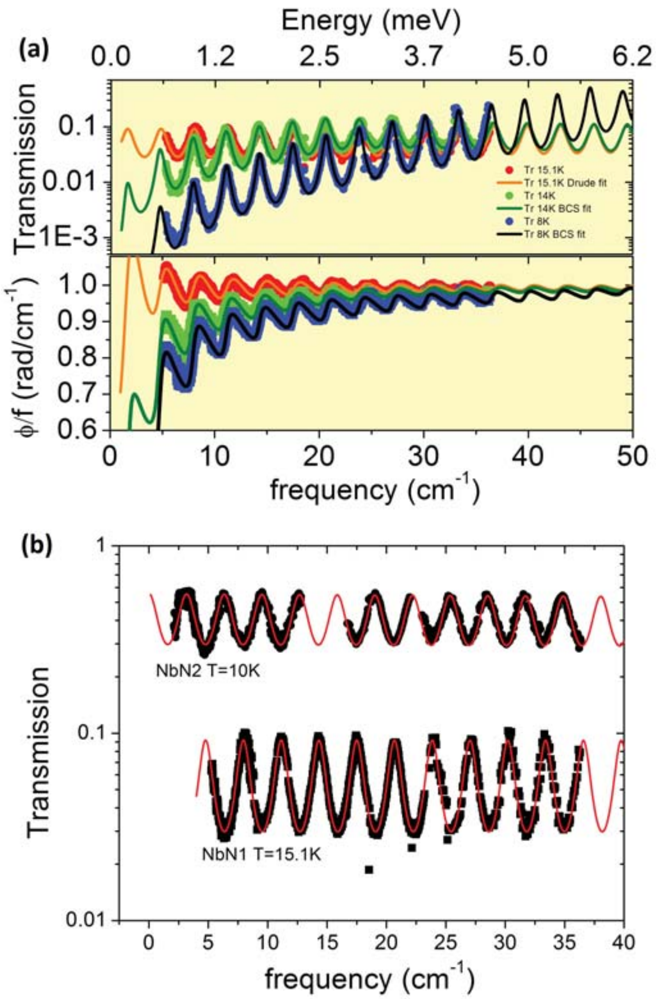

Figure 2.5: **(a),** "raw" data as obtained from the THz frequency-domain Mach-Zehnder interferometer on an NbN sample with $T_C = 15.1K$ at temperatures above and at T_C. The observed oscillation results from the multireflection of the radiation on the edges of the substrate, also known as Fabry-Perot oscillation. Upper panel shows the transmission of versus frequency and energy. Lower panel shows the phase shift over frequency as a function of frequency and energy. The decrease in Transmission reflects the decrease in σ_1 while the decrease in ϕ/f reflects the increase of σ_2 ($\sigma_2 \propto 1/\omega$). The thick curves are the measurements and thin curve is a fit to BCS (Zimmermann equation, see text). At $T = T_C$ the thin curve is a fit to Drude model. **(b),** the transmission at $T > T_C$ of a highly disordered NbN sample ($NbN2$, with $T_C = 4.2K$) and a low disordered NbN sample ($NbN1$, with $T_C = 15.1K$, shown in (a)). Note the significant difference between the low and high disorder samples and the fact that the highly disordered sample is almost transparent, i.e. Transmission = 1.

Chapter 3

Results and discussion

3.1 Tunneling measurements across the d-SIT

The current section briefly summarizes the results and discussion presented in the attached papers: paper 6.1 and paper 6.2. Employing a planar tunneling junction arrangement, as sketched in Fig.2.3(b), the density of states of a superconducting and an insulating InO samples were measured. Measuring the global resistance versus temperature of these films, as sketched in Fig.2.3(a), revealed that the insulating sample followed an Arrhenius law (see Eq.1.8) with $T_0 \sim 0.4K$ $(0.034meV)$ and in the superconducting sample $T_C \sim 3K$. The most important and rather unexpected observation is that for both the insulating and the superconducting samples the extracted value of Δ from the tunneling conductance is $0.7meV$. This result provided the first direct experimental evidence for a superconducting gap in an homogeneously disordered uniform insulating sample. Indirect evidence for the survival of superconducting correlations in the insulating side of the d-SIT were presented previously in the review section. The evolution of superconducting gap was also measured as a function of magnetic field for both the insulating and the superconducting samples. Interestingly the similarity between these two samples extends even further. First Δ seems to vanish at a similar magnetic field. Secondly, at a high magnetic field, where the superconducting correlations are wiped out or at energies above Δ for any magnetic field strength, the tunneling density of states of both films follows Altshuler-Aronov expression of a logarithmic depletion around E_f (see Eq.1.4). Equally interesting is the appearance of the so called coherence peaks also in the insulating sample. This implies that coherent superconductivity is present in a sample with a global insulating transport behavior; hence, it strongly supports the idea of disorder induced electrical granularity. It is worth mentioning here that a similar picture, i.e. the survival of Δ across the SIT, was experimentally obtained in the case of granular films, as shown in Fig. 1.10(c)&(d).

3.2 THz spectroscopy measurements on disordered superconductors

The current section reviews and extends our results and discussion presented in the attached paper: 6.3. The prime theory describing the response of an s-wave superconductor at finite frequency was brought forward by Mattis and Bardeen[78]. Their expression was developed based on the BCS theory. One of the most useful expression introduced in their work predicts the behavior of the complex conductivity as a function of frequency and temperature, i.e. $\sigma_1(\omega, T)$ and $\sigma_2(\omega, T)$. Our measurements on NbN films far from the d-SIT, as seen in Fig 3.1, revealed an excellent agreement with the Mattis-Bardeen equations. In order to describe the electrodynamics of superconductors, different length scales should be considered as their relative values determines the response to the electromagnetic field. The first length scale is the London penetration depth: $\lambda_L = \sqrt{\frac{c^2}{4\pi\sigma_2(\omega)\omega}} = \sqrt{\frac{mc^2}{4\pi N_s e^2}} = \frac{c}{\omega_p}$, where m and e are the electron mass and charge, N_s is the superfluid density, c is the speed of light and ω_p is the plasma frequency. The second length scale is the correlation length: $\xi_0 = \frac{\hbar v_F}{\pi\Delta}$, which roughly describe the spatial length scale of the Cooper pairs. The third length scale is the mean free path of the normal state electrons: $l = v_F\tau$, which is set by the impurities and lattice imperfections at low temperatures. For typical metallic superconductors these three length scales are of the same order of magnitude. The local limit is when $l << \xi, \lambda$; more commonly referred to as the dirty limit defined by $l/\xi \to 0$. The opposite limit, is the so called clean limit $l/\xi \to \infty$, where it is necessary to distinguish the following two cases: the non-local (or Pippard) limit define by $\lambda << \xi, l$ and the local (London) limit defined by $\xi << \lambda, l$ (also known as the regime of type II superconductors). With increasing disorder the penetration depth increases and the coherence length and mean free path decreases. Indeed, the disorder InO and NbN films are in the local limit. In principle, Mattis-Bardeen equations are not applicable in the local limit. In 1991 Zimmermann et al.[93] extended Mattis-Bardeen expressions to any degree of disorder. Hence we employed these latter expression through out the text and refer to them as BCS theory.

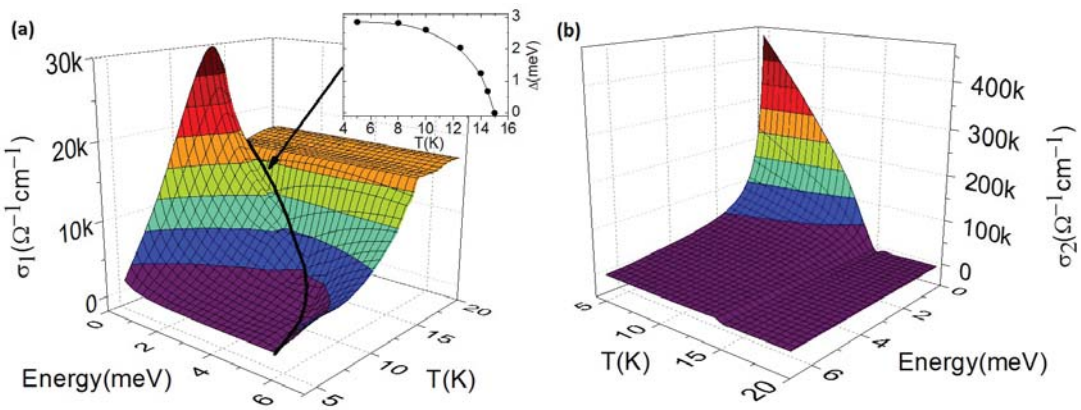

Figure 3.1: **(a)**, the measured real part of the complex conductivity as a function of photon energy and temperature, $\sigma_1(\omega, T)$, for the 'cleanest' NbN film with a $T_C = 15.1K$. The results perfectly fit Mattis-Bardeen equations. The blacked line (min$[\sigma_1(\omega)]$) corresponds to the value of the superconducting energy gap, and is plotted separately in as a function of T together with a fit the BCS theory (which predicts the evolution of Δ with T). The pronounced maximum at low frequencies and at a temperature slightly below T_C is the coherence peak[89]. **(b),** the measured imaginary part of the complex conductivity as a function of photon energy and temperature, $\sigma_2(\omega, T)$, for the same sample.

The general shape of $\sigma_1(\omega)$ and $\sigma_2(\omega)$ according to Zimmermann, however, remains unaffected. Moreover, it can also be understood by the following phenomenological arguments. Fig. 3.2 shows the evolution of the density of states of a superconductor above and below the critical temperature, T_C. Probing such a system held above T_C enables the excitations of single-particles from occupied states to empty states for any finite photon energy. This scenario ultimately leads to a Drude response, where the two important parameters are the dc conductivity σ_{DC} and the scattering rate of normal electrons τ. Reducing the temperature below T_C effects the complex conductivity due to the opening of an energy gap (see Fig.3.2(b)) and condensation of electrons into Cooper pairs. At frequencies much higher than the pair breaking energy, 2Δ, σ_1 still determined by the normal state electrons; however when the photon energy decreases and there are less possible transitions across the gap σ_1 decreases until reaching a minimum at $\hbar\omega = 2\Delta$. At even lower frequencies σ_1 increases due to the broadening of the δ-function at $\sigma_1(\omega = 0)$ or σ_{dc}. The latter quantity is related to the divergence of σ_2, which is proportional to $1/\omega$, according to Kramers-Kronig relation. At zero temperature σ_1 will be zero $\forall : \hbar\omega < 2\Delta$. This description of the behavior of the complex conductivity can be observed in Fig.3.1, which we obtained from a clean NbN sample.

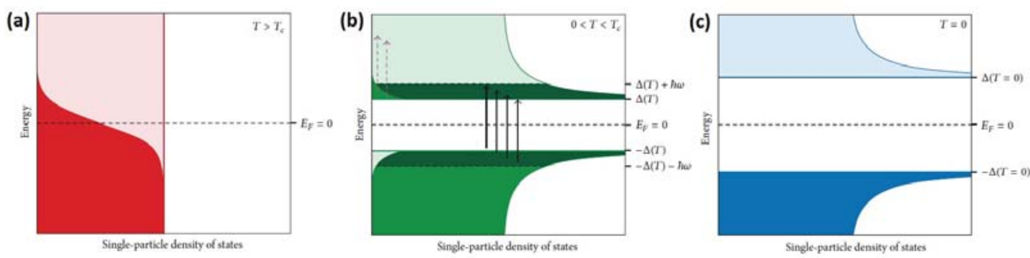

Figure 3.2: The density of states in the vicinity of the Fermi energy. **(a)**, for a normal metal. The dark colored area indicates the occupied states according to the Fermi-Dirac statistics at finite temperatures. Clearly any photon energy can excite electrons from an occupied state to unoccupied state. **(b)**, for a superconductor at finite temperature an energy gap is opened around the Fermi energy. In this case there are two possible excitations; first across the gap (solid arrows) for $\hbar\omega > 2\Delta(T)$ and second from those above the gap between occupied and unoccupied states due to the finite temperature Fermi distribution. **(c)**, at zero temperature latter mechanism is no longer available and the only optional excitation is across the superconducting gap. Adopted from ref.[89]

There are several fundamental differences between the intensively explored dc measurements and the THz free-spacee spectroscopy measurements we employed. In the first place, the optical method uses a macroscopic beam diameter. Moreover the radiation wavelength goes to infinity in the direction parallel to the films surface since the k-vector of the transmitted radiation is perpendicular to the films surface. Thus, unlike dc measurements, such an optical probing is not sensitive to percolations paths within the disordered film nor it is sensitive to specific energetically preferred tunneling channels in to the disordered films. In the second place optical probing and dc probing (tunneling or transport) are basically measuring different responses. Optical spectroscopy measures the complex response function of the film, for example the conductivity which is the current-current correlation function, by measuring the films absorption and scattering of the emitted photons. Whereas dc measurements like tunneling is based on injecting electrons into the films. Hence, the observed Altshuler-Aronov like depletion in the tunneling density of states around the Fermi energy, as seen in Fig. 4 paper 6.1, is not expected to appear (by any sort) in an optical probing. On the other hand, collective modes, discussed in chapter 4 are not visible in the single electron tunneling density of states. These differences between the two methods can be used further to shed light on the physics of the SIT in a number of ways. Paper 6.3 compares results from tunneling and optical measurements on InO films. It mainly relies on a sort of technical difference between the two methods. Tunneling measurements naturally requires an adjacent metal plane to inject electrons through a thin barrier. The metallic plane screens the Coulomb interactions within the disordered sample. Whereas in the optical setup no such metal plane exist close to the film. In view of these results we continue to explore the effect of screening, as details in section 3.3.1.

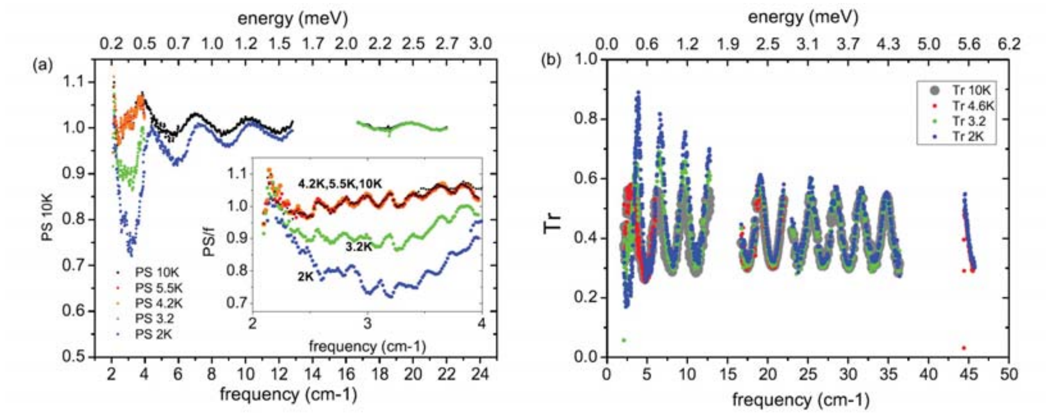

Figure 3.3: **a**, phase shift over photon energy versus photon energy. The deviation downward of the observed Fabry-Perot oscillations at low frequencies below T_C indicates the $1/\omega$ divergence of σ_2, which is proportionall to the superconducting electron pair density or superfluid stiffness. **b**, the corresponding transmission versus photon energy. **c**, the transmission versus photon energy for the same film shown in (a)&(b) together with the result from the cleanest NbN film, having a T_C of $15.1K$.

Particularly interesting is the value of the conductivity of such disordered films in the vicinity of the SIT. Fig. 3.3 show the THz measurement 'raw data', i.e. the transmission versus photon energy and the phase shift divided by photon energy versus photon energy. Using Fresnel equations the complex conductivity can be extracted without any extrapolation (e.g. Kramers-Kronig relation) or the a priori assumption of any physical model. At temperatures slightly above T_C the results aduquetly fit Drude, which is written as follow: $\sigma(\omega) = \frac{Ne^2\tau}{m}\frac{1}{1-\omega\tau} = \sigma_{dc}\frac{1+i\omega\tau}{1+\omega^2\tau^2}$, where N is the electron density, m and e are the electron's mass and charge, τ is the scattering rate and ω is the photon energy. There are two fitting parameters to Drude model, the first is the scattering rate,τ, and the second is the dc conductivity, σ_{dc}. The value of τ can not be determined for the films we studied with our THz system since it resides at a much higher frequency than our spectrum. In general the scattering rate increases with disorder and even for our cleanest samples the conductivity above T_C seems flat, as seen in Fig.3.1(a), indicating that the scattering rate is faster than our probing frequency[1]. Nevertheless, the actual value of τ does not impair our fitting with an effective one parameter, namely σ_{dc}. For the highly disorder NbN shown in Fig. 3.3(a)&(b) we obtain $\sigma_{dc} = 1100\Omega^{-1}cm^{-1}$ slightly above T_C. Translating this value[2] to R_{sq} we obtain a value of $54k\Omega$, already much higher than the transport measured σ_{dc}. This discrepancy apparently support the notion of electrical granularity, otherwise in an homogeneous sample we expect to retrieve similar results to those obtained in transport measurements.For our lowest disordered sample the corresponding result gives $R_{sq} = 350\Omega$ or $\rho = 60\mu\Omega^1 cm^1$, similar to the transport results.

[1]The actual value of scattering rate was inferred by extrapolation in previous microwave measurements[75] to be in the order of $200 - 300THz$.

[2]The samples are squared, hence: $R_{sq} = \frac{\rho l}{A} = \frac{0.9\times10^{-3}\times10^{-2}}{17\times10^{-9}\times10^{-2}} = 5.3\times10^4\Omega = 5.3\times10^4\frac{\Omega}{square}$.

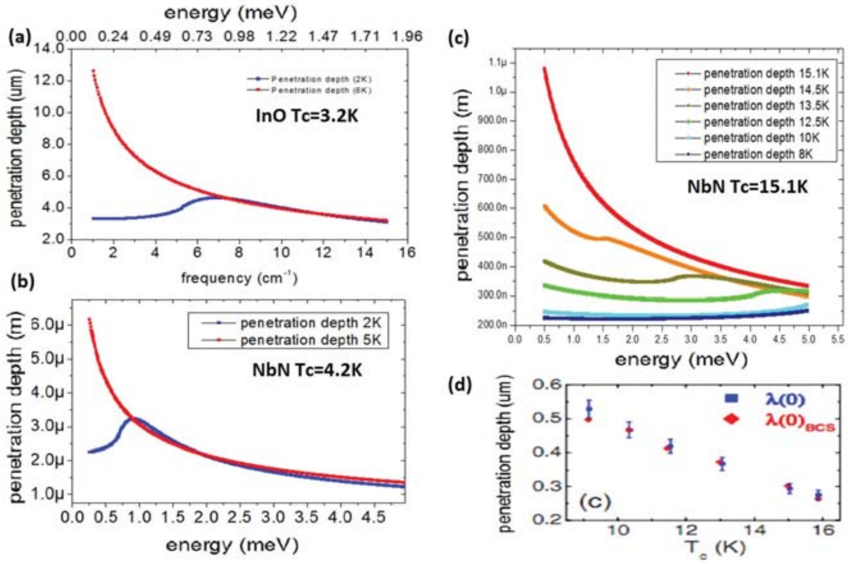

Figure 3.4: **a**, the penetration depth versus photon energy of a superconducting InO sample at temperatures below ($2K$) and above ($6K$) the critical temperature ($3.2K$). **b**, the penetration depth versus photon energy of a superconducting NbN sample at temperatures below ($2K$) and above ($5K$) the critical temperature ($4.2K$). **c**, the penetration depth versus photon energy of the cleanest measured NbN sample at various temperatures. **d**, the penetration depth as obtained from a two-coil experiment performed on similar NbN films with relatively low disordered NbN films. Adopted from ref. [94].

The London penetration depth can also be estimated[74] based on our THz measurements results using the following relation: $\lambda_L = \sqrt{\frac{c^2}{4\pi\omega\sigma_2}}$. Fig. 3.4 show our results for a few selected InO and NbN samples alongside result from a two-coil experiment on similar, though low-disordered, NbN samples[94]. Apparently both our THz and the two-coils measurements results seem in good agreement. These two techniques, although completely different, shares a few important properties: they are both a global measurement (undependent of percolation paths) and are both measuring an unperturbed sample (in a sense that there are no metallic plane screening the Coulomb interactions). In principle the superconducting gap can be extracted from the behavior of the penetration depth versus temperature curves. However, there is not much sense in doing so in our case since the extracted value ultimately rely on the exact same data that leads in a more direct way to the same value, i.e. via the minimum in σ_1. In case we consider other mechanism that derive σ_1 to a minimum (like the Higgs mode) it still make no sense to use the penetration depth to extract the superconducting gap since the a priori model to achieve this value is no longer valid.

A few disordered InO samples were measured in an optical cryostat with a parallel magnetic field of up to $7T$. This special optical cryostat, however, is less suited for measuring the low spectrum of the THz system. At these long wavelengths the unavoidable mechanical imperfections of the systems are causing significant disturbances to the measured signal. Nevertheless, averaging over several measurements and employing other techniques to reduce standing waves may yield adequate results. Once the technical problems are resolved such a measurement may provide interesting data on the superconducting energy gap as a function of magnetic field. Moreover, it may be interesting to follow the complex conductivity of such films for which dc transport measurements reveal a magneto resistance peak. Such a pronounce behaviour is not expected in the optical measurements if indeed the magneto resistance peak is driven by the percolation picture described in Section 1.3.1. That is since all the relevant length scale in the optical measurement are macroscopic, the radiation beam diameter is a few millimeters and the radiation wavelength is in the submillimeter regime[3]

3.3 Unpublished results and suggestions for future work

3.3.1 The effect of Coulomb interaction on disordered superconductors

As was mentioned in the experimental section, the measurement of the tunneling density of states of disorder samples, where electron-electron interaction play an important role, are inherently problematic. The presence of an adjacent metallic electrode may screen the electron-electron interactions in the studied sample, thus alter the measurement results. The influence of a metallic plane is not restricted solely to the density of states of the studied sample, the transport behaviour is also affected. Paper 6.3 discuss the importance of Coulomb interactions in such disordered films. Here we present a complementary study. We measured the transport characteristics of couples of identical InO samples which were evaporated simultaneously. However, one sample was deposited on top of an insulating substrate whereas the other sample was evaporated on an surfaced oxidized Al film. We call the first a bare sample and the latter a screened sample. The purpose of this experiment is to detect the extent of the effect of screening on such homogeneously disorder and low carrier density films of InO. Fig.3.5(a-c) shows the resistance per square versus temperature ($R_{sq}(T)$) curves for couples of screened and bare samples. Clearly the presence of an adjacent metallic plane affects the $R_{sq}(T)$ curves. The screened samples exhibit enhanced superconductivity comparing to the bare samples. Especially interesting is the samples close to the d-SIT, where the bare sample exhibits an insulating trend whereas the screened sample exhibits a superconducting trend. Evidently, screening the Coulomb interactions can tune the quantum phase transition. The differences between these pairs continues also in the insulating side. Fig.3.5(e) shows a pair of insulating samples; the screened sample fits better the VRH resistance while the fits better the an Arrhenius low.

3.3.2 Resistance versus temperature curves

The definition of the superconducting critical temperature in homogeneously disordered films is not clear as in normal metallic superconductors. In the latter case, the superconducting fluctuations persist only over a very short temperature range. Increasing disorder extends the temperature range in which superconducting fluctuation play an important role. Two different theories calculated the effect of superconducting fluctuations around T_C on the films conductivity, namely Maki-Thompson (MT) and Aslamasov-Larkin (AL) corrections. The AL contribution for a $2D$ system is: $\sigma_{dc}^{2D-AL} = \frac{e^2\epsilon^{-1}}{16\hbar t}$ and for a $3D$ system: $\sigma_{dc}^{3D-AL} = \frac{e^2\epsilon^{-1/2}}{32\hbar\xi_0}$, where t is the thickness, ξ_0 is ground state coherence length and $\epsilon = |T/T_c - 1|$. The MT contribution for a $2D$ system is: $\sigma_{dc}^{2D-MT} = \frac{e^2 ln(\epsilon/\delta)}{8\hbar t(\epsilon-\delta)}$ and for a $3D$ system: $\sigma_{dc}^{3D-MT} = \frac{e^2\epsilon^{-1/2}}{8\hbar\xi_0}$ where δ is the pair-breaking parameter introduced to avoid an unphysical divergence of the conductivity at $T > Tc$ in the 2D case. Fig. 3.6(a) shows a typical resistance versus temperature curve for superconducting InO films. The behaviour of

[3]Though the radiation wave vector is perpendicular to the surface of the studied thin film, thus the radiation wavelength parallel to the film's surface is theoretically infinity.

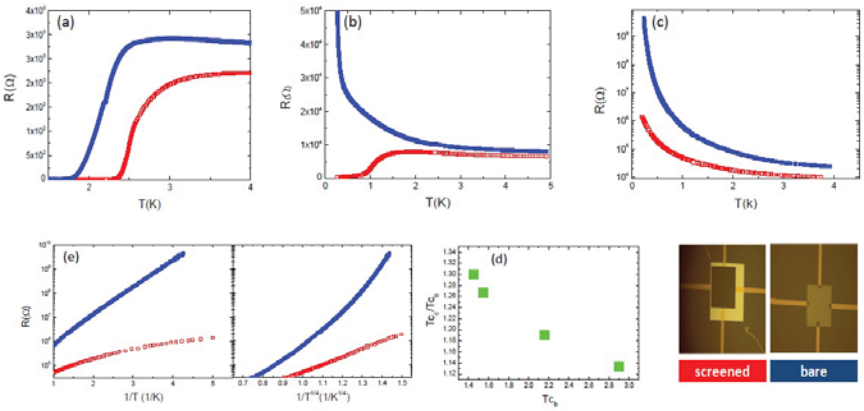

Figure 3.5: Resistance versus temperature for pairs of bare samples (blue full symbols) and capped samples (red open symbols) in three disorder limits: (a) both samples are on the superconducting side of the SIT, (b) the bare sample is insulating and the capped sample is superconducting and (c) both samples are insulating. (d) The ratio between the critical temperatures of both samples as a function of disorder manifested by the critical temperature of the bare sample for different pairs. (e) Log of the resistance versus $1/T$ (left) and $1/T^{1/4}$ (right) for the insulating sample of panel (c). Image on the right bottom side shows a pair of bare and capped samples, each connected by four ohmic contacts.

the $R(T)$ curve between the points where $dR/dT = 0$ and $R = 0$ can not be reconcile with either AL or MT corrections. In the relatively ordered InO sample shown here, the temperature that corresponds to the point where $dR/dT = 0$ is $\sim 30\%$ larger than the highest T_C found in literature for such homogeneously disordered InO; moreover, a local minimum in dR/dT curve can be seen in a temperature that is $\sim 85\%$ larger than the highest reported value of T_C. This demonstrates that superconducting correlations emerge at significantly higher temperatures. The emergence of the psedugap observed (see Fig. 1.12) in such InO samples occurs at temperatures corresponding to $dR/dT = 0$. Fig. 3.6(b) shows a similar picture obtained from a highly disordered NbN film. In view of the previous subsection, it would be interesting to give special attention to the differences in the $dR/dT = 0$ and the local minimum in dR/dT between screened and bare samples. Clearly the physical nature of the system in this temperature region should be further studied.

3.3.3 Tunneling with gating

Recently, the SIT in InO was tuned by gating the sample and consequently varying the electrons carrier density[95]. Ionic liquid was employed as the dielectric material between the sample and the metallic gate electrode. The huge dielectric constant of the ionic liquid enables to vary the carrier density up to $7 \times 10^{14} cm^{-2}$. In order to produce a significant change within the bulk sample it is necessary to have an ultra thin film, in the range of several nm, whereas most of the studied indium oxide samples describe here are thicker (few tens of nm). Apart from the dramatic change in the transport properties, a systematic variation of the magnetoresistance peak was studied and it seems to agree with a model which consists from electrical granularity. Merging the same gating procedure on a planar tunneling junction arrangement (see tunneling method) we studied the evolution of the tunneling density of states as a function of carrier density. Our results are incomplete and this work was stopped before reaching a solid ground. Nevertheless, the partial

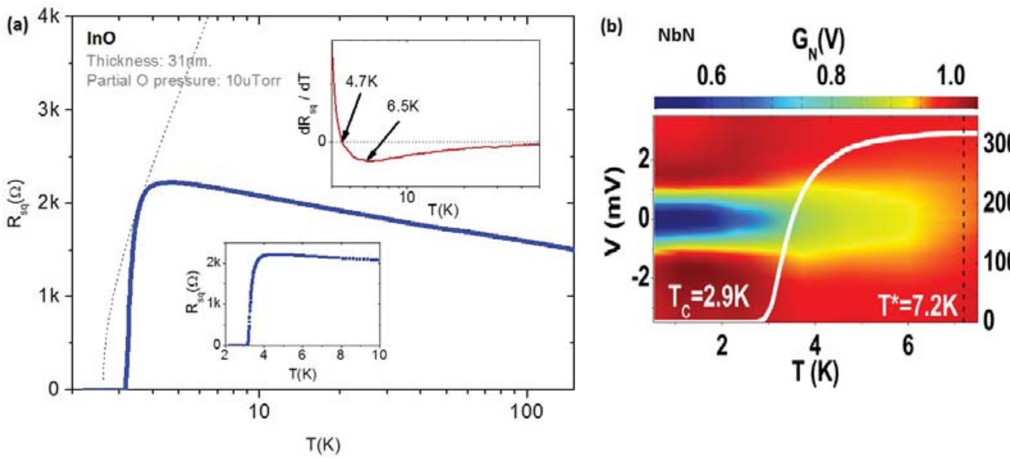

Figure 3.6: **(a),** Resistance per square versus temperature (on a log scale) for a superconducting InO film with a thickness of $31nm$. The partial oxygen pressure during the evaporation was $10\mu Torr$. The dashed line is a fit to Aslamasov-Larkin correction, which agree in a small region in the vicinity of T_C; clearly it can not explain the behavior of the curve. The lower inset shows the same result at low temperatures. The upper inset shows the derivative of the resistance in respect to temperature. Note that a minimum is observed at $6.5K$, much above the sharp decrease in resistance observed at $3.5K$. The derivative change sign in $4.7K$. **(b),** characteristic $R(T)$ (white curve) for a disordered thin NbN film with $T_C = 2.9K$. The background colors represents planar tunneling conductance, G. Note that the $R(T)$ decreases from as early as $T \sim 7.2K$; the latter temperature roughly signals the appearance of the pseudogap in the G data. Adopted from ref.[71]

data of the resistance versus temperature and the corresponding tunneling data is presented in Fig. 3.7. Evidently, despite the noisy experimental results, the superconducting gap persists also in gating voltage values which corresponds to $R(T)$ curves that do not show superconductivity. This result agree with the observations of paper 6.1 and paper 6.2.

3.3.4 Parallel magnetic field

Detecting the value of the superconducting gap is of great importance. In previous sections we reviewed the various experimental methods to detect it. However each method, especially in the case of highly disordered superconductors, does not necessary provide the true physical nature of the system due to different reasons. In the tunneling measurement the adjacent metallic electrode may screen the electron-electron interactions and in turn influence the value of Δ at the small area in which the electron tunnel. In the THz measurement, the highly disordered samples are almost transparent; consequently, the effect of superconducting correlations are small and the inferred value of Δ is less accurate. The necessity to measure the value of Δ is even more immediate given the disagreement between the THz and the tunneling measurements (as discussed in the next chapter).

The value of Δ might be recovered via a simple transport measurement. Applying a parallel magnetic field on a thin film will not induced vortex lines penetrating the sample. However it will, eventually, lead to an abrupt or gradual (depending on the electrical homogeneity) vanish of the superconducting gap, Δ. This will happen when the Zeeman energy exceeds Δ. In fact, this might be relevant to the Pauli paramagnetism limit (see ref.[96]): $H_P = \Delta/(2.82\mu_B)$, where

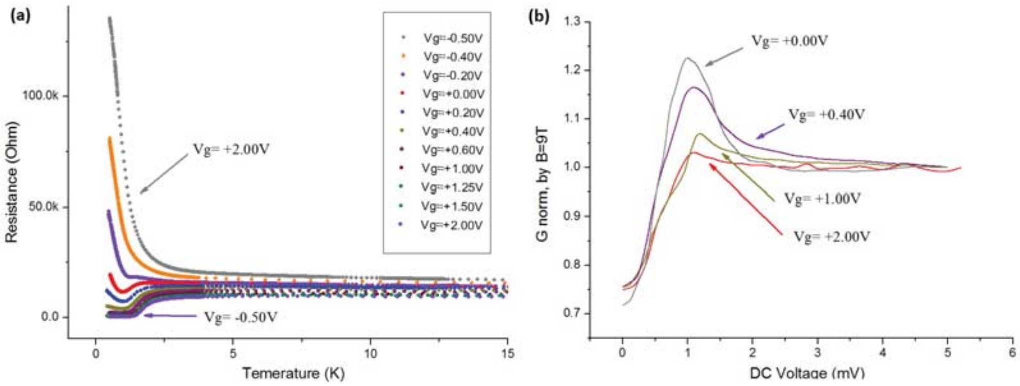

Figure 3.7: **a**, resistance versus temperature for different gating voltage on a superconducting ultra thin ($11nm$) indium oxide sample. Positive voltage deplete electrons from the gated area covering the junction, whereas negative voltage attracts electrons. Evidently, a ground state phase transition is observed with gating voltage. The reentrant behavior observed at the in between gating voltages might indicates on non homogeneous film structure, unlike the describe property of such films in this thesis. However, unlike the 'usual' InO film this specific film had a much lower thickness. **b**, tunneling density of states obtained at zero magnetic field and normalized to the $B = 9T$ corresponding results for several gate voltage values. For all gate voltage values a similar superconducting gap is apparent. While the so called coherence peaks seem to vanish with increasing gate voltage (decreasing electron carrier density).

μ_B is Bohr magneton (equals to $5.78 \times 10^{-5} eV/T$) and H_P may be associated with the magnetic field strength that corresponds to the emergence of resistance. Fig.3.8 shows the resistivity versus parallel magnetic field. Using the arguments mentioned here we obtain a superconducting energy gap value which matches the tunneling results.

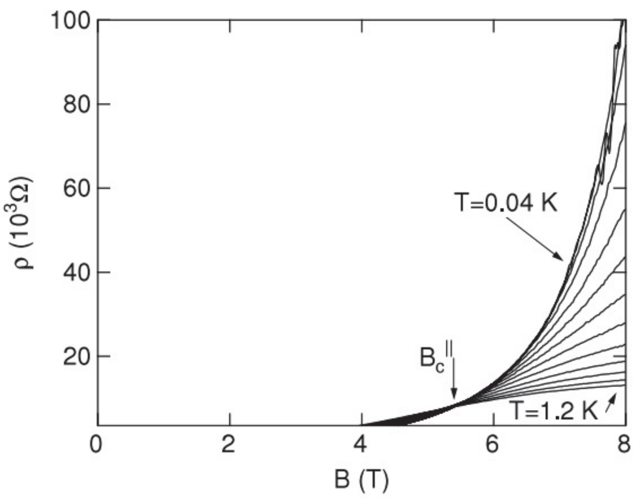

Figure 3.8: Sheet resistance, ρ, as a function of parallel magnetic field of an InO thin film at various temperatures ranging from $T = 0.04K$ to $T = 1.2K$. B_c marks the observed SIT; a value which is significantly higher than the critical perpendicular field. Adopted from ref. [97].

Chapter 4

Higgs mode near the d-SIT

Spontaneous breaking of continuous U(1) symmetry, is expected to yield two types of collective excitations: a gapless Nambu-Goldstone (phase) mode and a gapped Higgs (amplitude) mode with a finite Higgs mass which has gained much attention lately in the context of the standard model of high-energy physics. While being unstable towards the decay into electron pairs in homogeneous superconductors, the Higgs mode is theoretically predicted to become stable and experimentally detecable in disordered s-wave superconductors close to a quantum critical point. We study superconducting films of NbN and InO close to the superconductor-insulator quantum phase transition by means of optical spectroscopy and both planar-tunneling and scanning-tunneling spectroscopy. Our results reveal that the threshold for absorption in the optical conductivity is suppressed relative to the gap scale measured by tunneling. In addition, we find that there is excess low energy absorption not attributable to the breaking of Cooper-pairs. This spectral weight can be assigned to the Higgs mode. Our experimental results are in qualitative agreement with the optical conductivity of disordered Josephson-junction arrays calculated by using quantum Monte Carlo methods. In contrast to homogeneous BCS superconductors, the vicinity of a quantum phase transition enables us to detect the Higgs mode as a critical energy scale.

A superconductor spontaneously breaks continuous $U(1)$ symmetry and acquires the well-known *Mexican hat* potential with a degenerate circle of minima described by the order parameter $\Psi = Ae^{i\varphi}$, see Fig. 4.1a. On general grounds, excitations from the ground state can be classified as transversal Nambu-Goldstone (phase) modes and massive longitudinal Higgs (amplitude) modes (see blue and red lines in Fig. 4.1a) in analogy to the Higgs boson of high-energy physics. Indications of the Higgs mode in correlated many-body systems have been found in one-dimensional charge-density-wave systems [98] and two-dimensional superfluid Mott-insulators [99]. In homogeneous, BCS superconductors the Higgs mode is short-lived and decays to particle hole (Bogoliubov) quasi-particles[100, 101]. Indeed, decaying Higgs modes were inferred recently by pump-probe spectroscopy with pulse times equal to $\hbar/\Delta$ in clean BCS-superconductors [102], where Δ is the superconducting energy gap. An important question is whether in tailored superconducting systems the Higgs mode can be stable in time and remain well-defined. Recently, it was suggested [103, 104] that the proximity of a quantum critical point in low-dimensional quantum many-body systems hinders the Higgs mode from fast decay. This implies that in superconducting thin films close to the superconductor-insulator quantum-phase transition (QPT) a long-lived and well-defined Higgs mode should be visible.

The desired QPT from a superconductor to an insulator can be achieved in a number of ways.

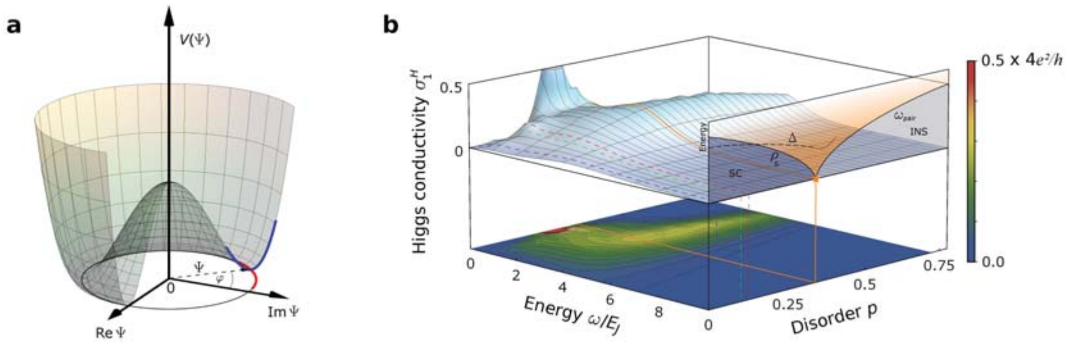

Figure 4.1: (Color online) **Broken $U(1)$-symmetry phase and quantum Monte Carlo calculation of the Higgs conductivity.a.** When symmetry is broken, the potential acquires a *Mexican hat* shape with a circle of potential minima along the brim (black solid circle). Transversal modes of the order parameter $\Psi = Ae^{i\varphi}$ along the brim (red line) are Nambu-Goldstone (phase) modes, and longitudinal modes (blue line) are Higgs (amplitude) modes associated with a finite energy. In superconductivity, the potential corresponds to the free energy. **b.** The Higgs mode gives rise to low-frequency conductivity (in units of $4e^2/h$), that grows as disorder p (fraction of disconnected superconducting islands) is increased and remains finite through the quantum phase transition (orange line). At the quantum critical point, $p_c = 0.337$, the superfluid density, ρ_s, in the superconducting phase vanishes and the quasiparticle gap, Δ, remains finite whereas in the insulator ω_{pair}, which is the energy to insert a Cooper-pair to the insulator, goes to zero. Results for specific disorder (blue, green, and red dashed lines) and compared to experiment, see Fig. 4.3. For details of the calculation see [105].

One is an array of superconducting islands embedded in an insulating matrix in which the transition is controlled by the ratio E_J/E_C, E_J being the Josephson coupling between islands and E_C the charging energy of an island [103, 104]. Another more practical way to drive a system through the QPT is by introducing disorder on atomic length scales. It has been shown both experimentally [20, 30, 71, 90] and theoretically [44, 46, 65] (and paper 6.1) that though being morphologically homogeneous, with increasing disorder superconducting films can progressively become electronically granular on length scales comparable to the superconducting coherence length. While for modest disorder the superconducting state is hardly affected, strong disorder near the quantum critical point decomposes the homogeneous state in individual superconducting islands. In this scenario, the QPT takes place at the critical disorder when phase fluctuations between different islands destroy the global phase coherence and the superfluid density ρ_s vanishes on a macroscopic length scale [50]. Consequently, the loss of global phase coherence does not necessarily cause the *pairing* gap Δ to close as the decoupled islands still remain superconducting. The value of the critical temperature T_c in the vicinity of the QPT is thus not defined by the opening of a gap in the quasiparticle density of states, but rather by the presence of a global phase coherence. Indeed, finite values of Δ in strongly disordered thin films were experimentally observed in tunneling spectroscopy experiments where T_c was already vanishingly small on the superconducting side or even zero on the insulating side of the QPT [73, 106](and paper 6.1). Near the QPT one expects two critical energy scales: in the insulating side, a charge gap ω_{pair}, which is the energy required to insert a Cooper-pair into the pair insulator [50], and in the superconducting side, the Higgs (amplitude) mass gap. Both energy scales should vanish at the QPT.

Assuming the presence of a Higgs mode in the superconducting thin film, what would be the most suited experimental quantity to detect it? The Higgs mode is a finite-energy oscillation of the order parameter magnitude $|\Psi|$. It can be probed by the dynamical conductivity $\hat{\sigma}(\omega)$ which depends on the current-current correlation function $\langle [j(t), j(0)] \rangle$. At low temperatures, the current is dominated by the Cooper pair current $j \sim (2e)\mathrm{Im}\{\Psi^* \nabla \Psi\} \simeq (2e)|\Psi|^2 \nabla \varphi$, where φ is the local phase field. As a result, the conductivity depends on a convolution of the amplitude and phase fluctuations.

How would the Higgs mode contribute to the dynamical conductivity? Theoretically it is predicted to give rise to excess conductivity at sub-gap frequencies [103] which we will refer to as *Higgs conductivity*, $\hat{\sigma}^H(\omega)$, in the remainder of the paper. In non-disordered systems $\sigma_1^H(\omega)$ shows a hard gap at frequencies similar to the superconducting gap, $\omega \sim 2\Delta/\hbar$, that is associated with the energy scale of the Higgs mode, m_H. This gap becomes softer as the system approaches the QPT, reaching zero at the critical point. Recently Swanson and collaborators [105] studied the effect of disorder on the dynamical conductivity across the superconductor-insulator QPT employing quantum Monte Carlo methods and extracted the excess low-frequency contribution, see Fig. 4.1b. The calculations show that the presence of disorder suppresses m_H so that $\sigma_1^H(\omega)$ remains finite across the QPT. This excess conductivity adds to the conductivity stemming from the superfluid condensate and the quasiparticle dynamics, so that one can write

$$\hat{\sigma}(\omega) = \sigma_1(\omega) + i\sigma_2(\omega) = \underbrace{A\rho_s\delta(\omega) + \hat{\sigma}^{qp}(\omega)}_{\hat{\sigma}^{\mathrm{BCS}}(\omega)} + \hat{\sigma}^H(\omega) \tag{4.1}$$

where ρ_s is the superfluid density and A is a constant,[74]. Even though m_H as a threshold energy scale can be smeared in the presence of disorder, its contribution to the spectral weight should be present and increase in magnitude as the system approaches the critical disorder, $p_c = 0.337$.

In order to experimentally search for the contribution of the Higgs mode, we have studied disordered superconducting films of NbN and InO by means of THz spectroscopy. Since the superconducting energy gaps are of the order of $0.1 - 1$ THz, optical spectroscopy in this regime is an alternative method to tunneling spectroscopy for the measurement of 2Δ. Most important, unlike tunneling which measures the density of states of the quasiparticles, optical spectroscopy probes a complex response function, $\hat{\sigma}^{\mathrm{exp}}$, that constitutes from the superfluid condensate, the quasiparticle dynamics and collective modes, see Eq. (4.1). One can decompose the optically measured conductivity into the regular BCS contribution and the contribution of the collective excitations. The first one is modeled by the Mattis-Bardeen theory for ordinary superconductors using our tunneling spectroscopy results as input to fix the absolute numbers. The difference to the experimental data determines the Higgs mode simply by calculating

$$\sigma_1^H(\omega) = \sigma_1^{\mathrm{exp}}(\omega) - \sigma_1^{\mathrm{BCS}}(\omega). \tag{4.2}$$

We have measured the complex transmission coefficient of several thin-film samples with different degrees of disorder utilizing Mach-Zehnder interferometry. Measurements were performed in the frequency domain between $0.05 - 1.2\,\mathrm{THz}$ ($0.18 - 5\,\mathrm{meV}$) for temperatures above and well below T_c. From this we directly obtain the real and imaginary parts, $\sigma_1^{\mathrm{exp.}}$ and $\sigma_2^{\mathrm{exp.}}$, of the dynamical conductivity, in a individual manner without Kramers-Kronig analysis. According to Mattis-Bardeen theory the minimum in $\sigma_1(\omega)$ equals to twice the superconducting energy gap, 2Δ. Furthermore, the superfluid density is related to $\sigma_2(\omega)$

$$\rho_s = \frac{\sigma_2(\omega) m \omega}{e^2} \tag{4.3}$$

where m is the electron mass and e is the elementary charge. This robust approach is well established to study superconducting thin films. For more details see the methods section and, e.g., [74, 86, 88, 107]. Fig. 4.2b,e shows the real part of the conductivity $\sigma_1^{\mathrm{exp}}(\omega)$ for modestly ($T_c = 9.4\,\mathrm{K}$) and strongly ($T_c = 4.2\,\mathrm{K}$) disordered NbN in the normal state and well below T_c together with the fits to Mattis-Bardeen prediction for the disordered regime [78, 93]. In both cases, $\sigma_1^{\mathrm{exp}}(\omega)$ is featureless in the normal state following simple Drude behaviour with a scattering rate well above the THz range, whereas $\sigma_1^{\mathrm{exp}}(\omega)$ is strongly suppressed in the superconducting state. The ordered sample is fitted perfectly by the Mattis-Bardeen theory. The onset of the high-frequency upturn coincides with twice the energy gap, Δ_t, obtained by tunneling spectroscopy performed on a similar sample [20]. The situation is remarkably different for the strongly disordered sample. Here the decrease towards low frequencies is not at all captured by theory (green curve). In fact, using Δ_t extracted from corresponding tunneling experiment yields a curve which is significantly below $\sigma_1^{\mathrm{exp}}(\omega)$. With increasing disorder, both the discrepancy between $2\Delta_t$ and $\min[\sigma_1^{\mathrm{exp}}(\omega)]$ and the insufficiency of Mattis-Bardeen fits become progressively worse. This trend is demonstrated in Fig. 4.2c where we compare results from both techniques on a large number of NbN and InO samples spanning the various degrees of disorder (measured in terms of the normalized critical temperature, $\tilde{T}_c = T_c/T_c^{\mathrm{clean}}$). For small disorder, $\tilde{T}_c \simeq 1$, tunneling and THz spectroscopy yield the same value for the superconducting energy gap. Upon increasing disorder (decreasing $\tilde{T}_c$) the discrepancy becomes more and more pronounced. For the most-disordered samples, we find about one order of magnitude difference between corresponding values. We assign these differences to an absorption process stemming from the Higgs mode that becomes progressively prominent as the system approaches the quantum critical point. This explains the discrepancy in the sense that $\min[\sigma_1^{\mathrm{exp}}(\omega)]$ in the strong-disorder limit does no longer equal 2Δ as a consequence of the additional conductivity $\sigma_1^H(\omega)$ of the emergent Higgs mode. The previously prominent spectral feature marking the gap frequency is now hidden in the shoulder at higher frequencies. Although a distinct experimental determination of $\min[\sigma_1^{\mathrm{exp}}(\omega)]$ becomes progressively difficult as it is pushed to low frequencies, we note the resemblance between $\min[\sigma_1^{\mathrm{exp}}(\omega)]$ and the theoretical prediction of m_H in the vicinity of the critical point [103], as seen in Fig. 4.2c.

We now explore the evolution of the observed additional excess weight associated with the Higgs conductivity, $\sigma_1^H(\omega)$, as defined in Eq. (4.2), and compare these measured results with recent numerical simulations detailed in ref. [105] and sketched in Fig. 4.1b. Fig. 4.3a shows the measured $\sigma_1^H(\omega)$ for three disordered NbN films with different $T_c = 6.7$, 5 and $4.2\,\mathrm{K}$ and the theoretical calculation for corresponding values of disorder $p = 0.075$, 0.1 and 0.125. We note that one cannot expect a perfect quantitative agreement since the theory assumes that 2Δ is much larger than the Higgs mode energy, whereas experimentally they are of the same order of magnitude. Nevertheless, the overall behaviour and even quantitative trends are shared by theory and experiment: There is a pronounced peak of $\sigma_H(\omega)$ that shifts towards smaller frequencies and becomes sharper with increasing disorder.

The appearance of the Higgs mode must go along with a redistribution of the spectral weight as this quantity is strictly conserved; it measures the total charge carrier density N in the system [74]. In accordance with the bosonic model of the SIT sketched above, the strength of the δ-peak, i.e. the superfluid density ρ_s, dwindles to zero in the vicinity of the quantum critical point. Fig. 4.3b displays ρ_s for disordered NbN films extracted from the imaginary part of the conductivity, using Eq. (4.3) and N in the normal state obtained from Hall measurements. While ρ_s is reduced by about 2 orders or magnitude with increasing disorder, N is much less affected. According to Ferrell-Tinkham-Glover sum rule [74] for the 'missing' spectral weight s between normal and superconducting states,

$$s = \int_{0^+}^{\infty} d\omega[\sigma_1^n(\omega) - \sigma_1^s(\omega)] \sim \rho_s, \tag{4.4}$$

a reduced superfluid density ρ_s upon increasing disorder leads to a reduced value of s. As the quasi-particle gap remains fairly unchanged with disorder, this necessarily causes the spectral weight contribution of the Higgs mode, $\int d\omega\sigma_1^H(\omega)$, to become more pronounced. Fig. 4.3c depicts the detected linear relation between the missing spectral weight, s, and the superfluid density, ρ_s, for several films with different degree of disorder, thus providing the self consistency of the above argument and eliminating the possibility of a redistributed spectral weight to higher frequencies (due, for example, to a sudden change in the scattering rate).

We conclude that the low-frequency absorption observed by optical spectroscopy originates from the Higgs mode in superconductors close to a quantum phase transition. As the system approaches the critical point, the energy scale for this mode decreases and its magnitude grows, exhibiting quantitative agreement with numerical simulations. Theoretically the Higgs mode are predicted to be gapped in the ordered limit and ungapped in the presence of disorder. Our experimental resolution does not allow us to determine whether these modes are indeed gapped close to the critical point, nevertheless we show that the overall excess conductivity depicted in the experimental results is consistent with the theoretical predictions. Such modes should be relevant to other types of bosonic superconductors such as granular systems and Josephson junction arrays. Indeed similar results were recently observed in granular aluminum systems close to the superconductor-insulator QPT [108]. An important question is the effect of electron screening on the superconducting properties in general and the Higgs mode in particular. Recently we have shown that a small discrepancy between 2Δ extracted from THz versus tunneling experiments could be ascribed to screening of Coulomb interaction by the tunneling electrode (see paper 6.3). However, it is unlikely that this effect can cause a difference of an order of magnitude as seen in fig. 4.2c. Furthermore, it cannot explain the growing incapacity of theory to describe the experimental $\sigma_1(\omega)$. The precise influence of disorder and interactions on the Higgs modes requires additional theoretical treatment. It is evident that the vicinity to the QPT offers a unique opportunity to study the nature of the low energy collective excitations in superconductors.

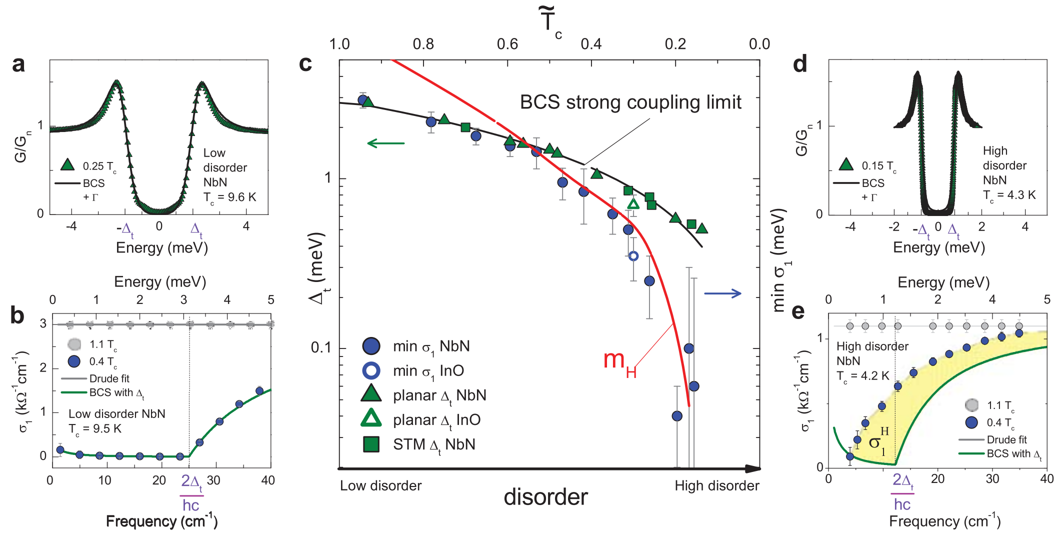

Figure 4.2: **Tunneling versus optical spectroscopy.** **a,b** Experimental results on low disordered NbN samples. Panel (a) shows the real part of the dynamical conductivity, σ_1, versus frequency (energy) at temperatures below and above $T_c = 9.5K$. The low temperature curve is fitted (green line) to Mattis-Bardeen while plugging in the energy gap value obtained in the corresponding tunneling result, Δ_t. Panel (b) shows the measured tunneling conductance spectrum (green triangles) alongside a fit to BCS (black line) with a Dynes broadening parameter, Γ. **c**, summary of the quasiparticle tunneling gap, Δ_t (green symbols), versus the $min(\sigma_1(\omega))$ (blue symbols) obtained from optical spectroscopy for several superconducting NbN and InO films spanning the different degrees of disorder. While the quasiparticle gap, Δ_t, remains fairly unchanged with increasing disorder and basically falls on the BCS strong coupling limit ratio, the minimum in $\sigma_1(\omega)$ is significantly suppressed. According to Mattis-Bardeen theory, for ideal superconductors the value of $\min[\sigma_1(\omega)]$ of the quasiparticle response corresponds to 2Δ. The discrepancy between both spectroscopic probes increases towards the highly disordered limit signaling the presence of additional modes superposing the quasiparticle response. The solid red line corresponds to the analytical prediction of m_H close to a QPT calculated by Podolsky et. al. [103].**d,e,** Experimental results on high disordered NbN samples. Panel (d) shows the real part of the dynamical conductivity, σ_1, versus frequency (energy) at temperatures below and above $T_C = 4.2K$. The low temperature curve is fitted (green line) to Mattis-Bardeen while plugging in the energy gap value obtained in the corresponding tunneling result. Unlike the case of the low disordered sample, these two curves different. The excess spectral weight, marked in yellow, defined as the difference between the curves and is attributed to the Higgs contribution, σ_1^H, see text. Panel (e) shows the measured tunneling conductance spectrum (green triangles) alongside a fit to BCS (black line) with a Dynes broadening parameter, Γ.

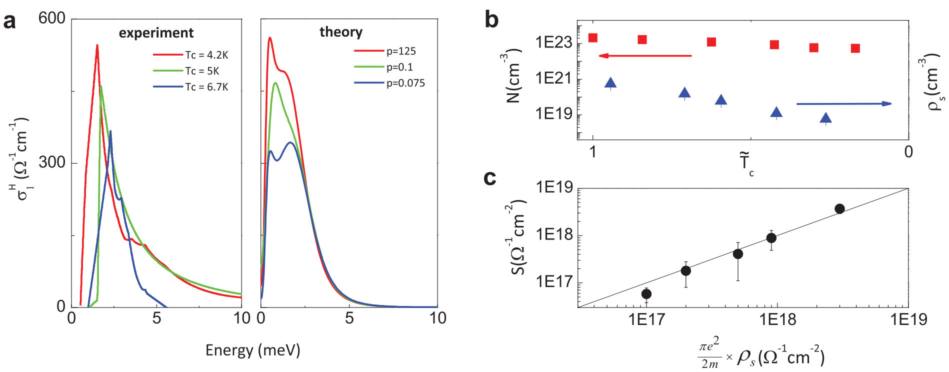

Figure 4.3: **Higgs conductivity and spectral weight.** **a**, Experimental and theoretical results for the Higgs conductivity σ_1^H as a function of energy for three NbN films of different disorder. The numerical results [105] were obtained for a fixed value of E_C/E_J, whereas the degree of disorder, reflecting breaking bonds between the superconducting islands, is denoted by p. Qualitative and quantitative features are shared by both experiment and theory. The sharp lines in the experiment data are due to extrapolation between measured data points. **b**, Charge carrier density N in the normal state obtained from Hall measurements (black squares) and superfluid density, ρ_s, measured by optical spectroscopy as functions of $T_c/T_c^{\rm clean}$ (reflecting the degree of disorder). Note the faster decrease of ρ_s with increasing disorder, indicating the vanishing contribution of the superfluid condensate to the spectral weight. **c**, the redistribution of the 'missing' spectral weight s between normal and superconducting state versus the superfluid density ρ_s, as defined in Eq. (4.4). The observed linear relation indicates that the redistribution of the spectral weight occurs within our measured energy spectrum.

Chapter 5

Discussion and summary

The set of experimental results presented here implies that an inhomogeneous electronic state emerges in a specific sort of homogeneously disordered superconducting systems. This experimental finding goes hand in hand with several theoretical predictions that adopted a model with an atomic scale disorder. Recently it was revealed in the case of the InO samples that there is a larger physical disorder scale, namely a compositional disorder. The scale or spatial fluctuations of carrier density might be the intrinsic modulator of the electrical inhomogeneity scale. It would be interesting to check whether compositional disorder exists in other films, particularly in TiN films, which shares with InO samples the set of results presented here[1], such as magneto resistance peak, spatially inhomogeneous order parameter, pseudo gap above T_C, simple activated behavior of the resistance versus temperature and a superconducting gap in the insulating side[2]. The commonality between the InO, TiN and to some extent the highly disorder NbN films is their low carrier density; which is at least an order of magnitude below normal metals. This intensifies the effect of electron-electron interactions and in turn affects the nature of the superconducting state. The theories that specifically discuss the emergent electrical granularity in homogeneously disordered films do not incorporate Coulomb interactions. We have shown experimentally the importance of these interactions in InO films by tuning the SIT with an adjacent metallic plane. By measuring tunneling we have shown (e.g. Fig.2 paper 6.1, Fig.5 paper 6.2) that the density of states of disordered InO in the vicinity of the d-SIT (from both sides) is suppressed due to electron-electron interactions. Embracing the disorder induced electrical granularity picture, the energy spacing in an individual grain is $\delta\epsilon = (g_0 b^3)^{-1}$, where g_0 is the density of states at the Fermi level in the bulk and b^3 is the average volume of one granule. Increasing Coulomb interaction suppresses g_0 and consequently the spacing between the energy levels grows. Equally important, the critical grain size, i.e. $b_{SC} = (g_0\Delta)^{-1/3}$, below which $\delta\epsilon > \Delta_{sc}$, increases. Hence, increasing disorder yields more stringent spatial conditions from an individual grain to superconduct and consequently hinders the large scale superconducting coherence. Clearly a more rigorous treatment is required to explore the way superconductivity is superimposed on a system where Coulomb interactions play an important role.

The resistance versus temperature curves also holds important information. The theories that discuss the emergent electrical inhomogeneity do not provide expressions for the reduction of T_C as a function of disorder, unlike the Fermionic model (which appears in good agreement for the

[1]To some extent NbN films also share many results with InO and TiN, however, the insulating phase of the NbN films do not exhibit an Arrhenius law

[2]For TiN films the existence of a superconducting gap was only inferred and was not directly observed

case of TiN films). On the other hand, the Fermionic picture do not incorporate spatial electrical inhomogeneity. The former theory seems to agree with several experimental results as discussed throughout this thesis, e.g. the magneto resistance peak. Embracing the phenomenological theory that describes the magneto resistance peak, we may attribute the temperature corresponding to $T(dR/dT = 0)$ to the state where percolation via the normal regions energetically equals to percolation via the superconducting regions. In that case the temperature at which the first superconducting island emerges is significantly higher than $T(dR/dT) = 0$. Interestingly, already the value of $T(dR/dT = 0)$ itself is significantly larger than the highest reported T_C. Apparently, the tunneling measurements, showing a psedugap significantly above T_C, support this picture. However, as we have shown by measuring screened and bare samples, tunneling measurements on such low carrier density may alter the results due to screening caused by the metallic electrode. Subsequently superconductivity may intensify in that specific region in which electrons tunnel into, while the remaining of the unperturbed film may have different electrical properties (e.g. lower T_C). This undermines to some extent the existence of such a pseudogap at temperatures much above T_C; While the arguments relying on the shape of the resistance and its derivative ultimately address an unperturbed system. Clearly further study of this subject is required.

Our initial goal from the THz optical measurement was to detect the superconducting gap close to the d-SIT and particularly in the insulating side and above T_C. We failed in these endeavors. In the insulating side and above T_C, where we believe that there is local superconductivity, the lack of global phase coherence hinders its detection with the optical method. close to the SIT from the superconducting side 2Δ is masks by the Higgs mode. The observation of the Higgs amplitude mode by our THz spectroscopy measurement is in some sense not entirely linked to the rest of the physics discussed here; perhaps because it is the first THz experiment on superconducting films with various degrees of disorder up till the d-SIT. Nevertheless, it is in the heart of such a quantum phase transition. We present the first experimental observation of a stable-in-time and well-defined Higgs mode in a superconducting system. This was possible by driving the superconductor close to quantum criticality, where the Higgs mode was expected to soften below 2Δ.

Chapter 6

Papers

6.1 Measurement of a Superconducting Energy Gap in a Homogeneously Amorphous Insulator

1

2

3

4

6.2 Tunneling Density of States of Indium Oxide Films Through the Superconductor to Insulator Transition

1

2

3

4

5

6

6.3 Effect of Coulomb Interactions on the Disordered-Driven Superconductor-Insulator Transition

1

2

3

4

5

6

7

8

Bibliography

[1] Anderson P W 1958 *Phys. Rev.* **109** 1492

[2] Mott N F 1967 *Adv. Phys.* **34** 1356

[3] Mott N F 1968 *J. Non-Cryst. Solids* **1** 1

[4] Mott N F 1993 *Conduction in Non-Crystalline materials 2nd edition* (Clarendon Press Oxford)

[5] Efros A L and Shklovskii B I 1975 *J. Phys. C.* **8** 49

[6] Altshuler B L, Aronov A, Gershenson M E and Sharvin Y 1987 *Sov. Sci. Rev. A* **9** 223

[7] Lee P and Ramakrishnan T 1985 *Rev. Mod. Phys.* **57** 287

[8] Bardeen J, Cooper L N and Schrieffer J R 1957 *Phys. Rev.* **106** 162

[9] Gorkov L 1959 *Sov. Phys. JETP* **9** 1364

[10] Anderson P 1959 *J. Phys. Chem. Solids* **11** 26

[11] Strongin M, Thompson R, Kammerer O and Crow J 1970 *Phys. Rev. B* **1** 1078

[12] Strongin M, Kammerer O F, Crow J E, Parks R D, Douglass D H and Jensen M A 1968 *Phys. Rev. Lett.* **21** 1320

[13] Graybeal J and Beasley M 1984 *Phys. Rev. B.* **29** 4167

[14] Graybeal J and Beasley M 1986 *Phys. Rev. Lett.* **56** 173

[15] Yazdani A and Kapitulnik A 1995 *Phys. Rev. Lett.* **74** 3037

[16] Gantmakher V, Golubkov M, Lok J and Geim A 1996 *JETP* **82** 951

[17] Hebard A and Paalanen M 1990 *Phys. Rev. Lett.* **65** 927

[18] Paalanen M, Hebard A and Ruel R 1992 *Phys. Rev. Lett.* **69** 1604

[19] Shahar D and Ovadyahu Z 1992 *Phys. Rev. B.* **46** 10917

[20] Chand M, Saraswat G, Kamlapure A, Mondal M, Kumar S and Jesudasan J 2012 *Phys. Rev. B.* **85** 014508

[21] Baturina T I, Mironov A Y, Vinokur V M, Baklanov M R and Strunk C 2007 *Phys. Rev. Lett.* **99** 257003

[22] Frydman A 2003 *Physica C* **391** 189

[23] Fukuzumi Y, Mizuhashi K, Takenaka K and Uchida S 1996 *Phys. Rev. Lett.* **76** 684

[24] Bollinger A T, Dubuis G, Yoon J, Pavuna D, Misewich J and Boovi I 2011 *Nature* **472** 458

[25] et al S H P 2001 *Nature* **413** 282

[26] Sondhi S, Girvin S, Carini J and Shahar D 1997 *Rev. Mod. Phys.* **69** 315

[27] Maekawa S and Fukuyama H 1981 *J. Phys. Soc. Jpn* **51** 1380

[28] Finkel'shtein A 1987 *JETP* **45** 46

[29] Hadacek N, Sanquer M and Villgier J C 2004 *Phys. Rev. B.* **69** 024505

[30] Sacepe B, Chapelier C, Baturina T I, Vinokur V M, Baklanov M R and Sanquer M 2008 *Phys. Rev. Lett.* **101** 157006

[31] Fisher M, Weichman P B, Grinstein G and Fisher D S 1989 *Phys. Rev. B.* **40** 546

[32] Fisher M 1990 *Phys. Rev. Lett.* **65** 923

[33] Fisher M, Grinstein G and Girvin S 1990 *Phys. Rev. Lett.* **64** 587

[34] Liu Y, McGreer K A, Nease B, Haviland D B, Martinez G, Halley J W and Goldman A M 1991 *Phys. Rev. Lett.* **67** 2068

[35] Jaeger H, Haviland D, Goldman A, Orr B and rrrrrapid comm 1986 *Phys. Rev. B.* **34** 4920

[36] Haviland D, Liu Y and Goldman A 1989 *Phys. Rev. Lett.* **62** 2180

[37] Orr B, Jaeger H, Goldman A and Kuper C 1986 *Phys. Rev. Lett.* **56** 378

[38] Jaeger H M, Haviland D B, Orr B and Goldman A M 1989 *Phys. Rev. B* **40** 182

[39] Steiner M A, Breznay N P and Kapitulnik A 2008 *Phys. Rev. B.* **77** 212501

[40] Markovic N, Christiansen C, Mack A M, Huber W H and Goldman A M 1999 *Phys. Rev. B.* **60** 4320

[41] Valles J M, Dynes R C and Garno J P 1992 *Phys. Rev. Lett.* **69** 3567

[42] ans JA Chervenak S H and JM Valles J 1994 *Phys. Rev. Lett.* **75** 132

[43] Kowal D and Ovadyahu Z 1994 *Solid State Comm.* **90** 783

[44] Ghosal A, Randeria M and Trivedi N 1998 *Phys. Rev. Lett.* **81** 3940

[45] Paramekanti A, Trivedi N and Randeria M 1998 *Phys. Rev. B.* **57** 11639

[46] Ghosal A, Randeria M and Trivedi N 2001 *Phys. Rev. B* **65** 014501

[47] Shimshoni E, Auerbach A, and Kapitulnik A 1998 *Phys. Rev. Lett.* **80** 3352

[48] Bulaevskii L N, Panyukov S V and Sadovskii M V 1987 *Sov. Phys. JETP* **65** 380

[49] Dubi Y, Meir Y and Avishai Y 2007 *Nature (London)* **449** 876

[50] Bouadim K, Loh Y L, Randeria M and Trivedi N 2011 *Nature Phys.* **7** 884

[51] et al M C 2012 *Phys. Rev. B.* **85** 014508

[52] Bishop D J, Spencer E G and Dynes R C 1985 *Solid St. Electron.* **28** 735

[53] et al T C 1981 *Phys. Rev. B.* **23** 6172

[54] HK Sin P L and McLean W 1984 *Phys. Rev. B.* **30** 4067

[55] Bergmann G 1976 *Phys. Rep.* **27** 159

[56] Givan U and Ovadyahu Z 2012 *Phys. Rev. B.* **86** 165101

[57] Dynes R, Garno J and Rowell J 1978 *Phys. Rev. Lett.* **40** 479

[58] DKowal and Ovadyahu Z 2008 *Physica C* **468** 322

[59] Cohen O, Ovadia M and Shahar D 2011 *Phys. Rev. B* **84** 100507

[60] Kopnov G, Cohen O, Ovadia M, Lee K H, Wong C C and Shahar D 2012 *Phys. Rev. Lett.* **109** 167002

[61] Stewart M, Yin A, Xu J M and Valles J M 2007 *Science* **318** 1273

[62] Hollen S M, Nguyen H Q, Rudisaile E, Stewart M D, Shainline J, Xu J M and Valles J M 2011 *Phys. Rev. B* **84** 064528

[63] Sambandamurthy G, Engel L, Johansson A and Shahar D 2004 *Phys. Rev. Lett.* **92** 107005

[64] Dubi Y, Meir Y and Aviahsi Y 2006 *Phys. Rev. B* **73** 054509

[65] Dubi Y, Meir Y and Aviahsi Y 2007 *Nature* **449** 876

[66] Shklovskii B I and Efros A L (eds)

[67] Butko V, DiTusa J and Adams P 2000 *Phys. Rev. Lett.* **84** 1543

[68] McMillan W L 1968 *Phys. Rev.* **167** 331

[69] Dynes R C, Narayanamurti V and Garno J 1978 *Phys. Rev. Lett.* **41** 1509

[70] Barber R P, Merchant L M, Porta A L and Dynes R C 1994 *Phys. Rev. B* **49** 3409

[71] Kamlapure A, Das T, Ganguli S C, Parmar J B, Bhattacharyya S and Raychaudhuri P 2013 *Sci. Rep.* **3** 2979

[72] Sacepe B, Chapelier C, T I Baturina V M Vinokur M R B and Sanquer M 2010 *Nature Commun.* **1** 140

[73] Sacepe B, Dubouchet T, Chapelier C, Sanquer M, Ovadia M, Shahar D, Feigelman M, and Ioffe L 2011 *Nature Phys.* **7** 239

[74] M D and Gruner G (eds) chap 1

[75] Crane R W, Armitage N P, Johansson A, Sambandamurthy G, Shahar D and Gruner G 2007 *Phys. Rev. B.* **75** 184530

[76] Liu W, Kim M, Sambandamurthy G and Armitage N P 2011 *Phys. Rev. B.* **84** 024511

[77] Liu W, Pan L, Wen J, Kim M, Sambandamurthy G and Armitage N P 2013 *Phys. Rev. Lett.* **111** 067003

[78] Mattis C and Bardeen J 1958 *Phys. Rev.* **111** 412

[79] Mondal M, Kamlapure A, Ganguli S C, Jesudasan J, Bagwe V, Benfatto L and ratap Raychaudhuri P 2013 *Sci. Rep.* **3** 1357

[80] Pan S H, O'Neal J P, Badzey R L, Chamon C, Ding H, Engelbrecht J R, Wang Z, Eisaki H, Uchida S, Gupta A K, Ng K, Hudson E W, Lang K M and Davis J C 2013 *J. Appl. Phys.* **114** 243905

[81] Matsunaga R, Hamada Y I, Makise K, Uzawa Y, Terai H, Wang Z and Shimano R 2013 *Phys. Rev. Lett.* **111** 057002

[82] Beck M, Klammer M, Lang S, Leiderer P, Kabanov V V, Goltsman G N and Demsar J 2011 *Phys. Rev. Lett.* **107** 177007

[83] Matsunaga R and Shimano R 2012 *Phys. Rev. Lett.* **109** 187002

[84] Pronin A, Pimenov A, Loidl A and Krasnosvobodtsev S I 1998 *Phys. Rev. B* **57** 14416

[85] Tashiro H, Graybeal J M, Tanner D B, Nicol E J, Carbotte J P and Carr G L 2008 *Phys. Rev. B* **78** 014509

[86] Pracht U, Scheffler M, Dressel M, Kalok D F, Strunk C and Baturina T I 2012 *Phys. Rev. B* **86** 184503

[87] Pronin A 2001 *Phys. Rev. Lett.* **87** 097003

[88] Pracht U S, Heintze E, Clauss C, Hafner D, Werner R B D, S Gelhorn M S, Dressel M, Sherman D, Gorshunov B, Ilin K S, Henrich D and Siegel M 2013 *IEEE Trans. on Terahertz Science and Technology* **3** 269

[89] Dressel M 2013 *Adv. Condens. Matter Phys.* **104379** 0

[90] Kowal D and Ovadyahu Z 1994 *Solid State Comm.* **90** 783

[91] Ping J, Yudhistira I, Ramakrishnan N and Cho S 2014 *Phys. Rev. Lett.* **113** 047206

[92] Chockalingam S P, Chand M, Jesudasan J, Tripathi V and Raychaudhuri P 2008 *Phys. Rev. B.* **77** 214503

[93] Zimmermann W, Brandt E, Bauer M, Seider E and Genzel L 1991 *Physica C.* **183** 99

[94] Kamlapure A, Mondal M, Chand M, Mishra A, Jesudasan J, Bagwe V, Benfatto L, Tripathi V and Raychaudhuri P 2010 *Appl. Phys. Lett.* **96** 072509

[95] Lee Y, Frydman A, Chen T, Skinner B and Goldman A 2013 *Phys. Rev. B.* **88** 024509

[96] Clogston A M 1962 *Phys. Rev. Lett.* **9** 266

[97] Johansson A, Shammass I, Stander N, Peled E, Sambandamurthy G and Shahar D 2011 *Solid Stat Comm.* **151** 743

[98] Sooryakumar R Klein M V R 1980 *Phys. Rev. Lett.* **45** 660

[99] Endres M, Fukuhara T, Pekker D, Cheneau M, Schau P, Gross C, Kuhr E D S and Bloch I 2012 *Nature (London)* **487** 454

[100] Sachdev S 1999 *Phys. Rev. B.* **59** 14054

[101] Zwerger W 2004 *Phys. Rev. Lett.* **92** 027203

[102] Matsunaga R, Hamada Y I, Makise K, Uzawa Y, Terai H, Wang Z and Shimano R 2013 *Phys. Rev. Lett.* **111** 057002

[103] Podolsky D, A A and Arovas D 2011 *Phys. Rev. B.* **84** 174522

[104] Gazit S, D P and Auerbach A 2013 *Phys. Rev. Lett.* **110** 140401

[105] Swanson M, YL L, M R and Trivedi N 2014 *Phys. Rev. X.* **4** 021007

[106] Mondal M, Kamlapure A, Chand M, GSaraswat, Kumar S, Jesudasan J, Benfatto L, Tripathi V and Raychaudhuri P 2011 *Phys. Rev. Lett.* **106** 047001

[107] Dressel M, Drichko N, Gorshunov B and Pimenov A 2008 *IEEE JSTQE* **14** 399

[108] Bachar N *unpublished*